



**JIMMA INSTITUTE OF TECHNOLOGY  
FACULTY OF MATERIAL SCIENCE AND ENGINEERING**

**EFFECT OF MAGNESIUM SUBSTITUTION ON THE  
STRUCTURAL, OPTICAL AND MAGNETIC PROPERTIES OF  
NICKEL-ZINC NANOFERRITE PREPARED BY SOL-GEL  
COMBUSTION METHOD**

**MSc THESIS**

**BY: MIHRET TEGEGN**

**JULY, 2021  
JIMMA, ETHIOPIA**

**JIMMA INSTITUTE OF TECHNOLOGY**  
**FACULTY OF MATERIAL SCIENCE AND ENGINEERING**

**EFFECT OF MAGNESIUM SUBSTITUTION ON THE STRUCTURAL,  
OPTICAL AND MAGNETIC PROPERTIES OF NICKEL-ZINC  
NANOFERRITE PREPARED BY SOL-GEL COMBUSTION METHOD**

**MSc THESIS**

**BY: MIHRET TEGEGN**

**UNDER THE GUIDANCE**

**OF**

**DR. PAULOS TADDESSE (Associate Professor)**

**DR. OLU EMMANUEL FEMI (Associate Professor)**

**A THESIS SUBMITTED TO THE FACULTY OF MATERIAL SCIENCE AND  
ENGINEERING OF JIMMA INSTITUTE OF TECHNOLOGY IN PARTIAL  
FULFILLMENT OF THE REQUIREMENTS FOR THE DEGREE OF  
MASTER OF SCIENCE IN MATERIAL SCIENCE AND ENGINEERING**

**JULY, 2021**  
**JIMMA, ETHIOPIA**

## **DECLARATION**

I, the undersigned, declare that this M.Sc. thesis proposal entitled “effect of magnesium substitution on the structural, optical and magnetic properties of nickel-zinc nanoferrite prepared by sol–gel combustion method” is my own original work and that has not been presented by me to any other university for similar or any other degree award.

Name: \_\_\_\_\_

Signature: \_\_\_\_\_

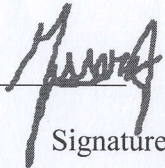
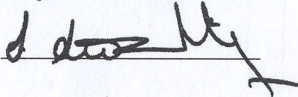

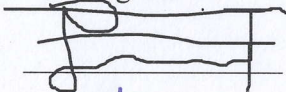

Date: \_\_\_\_\_

**JIMMA UNIVERSITY**  
**JIMMA INSTITUTE OF TECHNOLOGY**  
**SCHOOL OF POST GRADUATE STUDIES**  
**FACULTY MATERIALS SCIENCE AND ENGINEERING**

**Effect of magnesium substitution on the structural, optical and magnetic properties  
of nickel-zinc nanoferrite prepared by sol-gel combustion method**

By  
**Mihret Tegegn**

**APPROVED BY BOARD OF EXAMINERS**

1.	<u>Dr. Tessera Alemneh W. (PhD)</u>		<u>12 / July / 2021</u>
	External Examiner	Signature	Date
2.	<u>Dr. S. Sathiesh Kumar</u>		<u>12 / Jul / 2021</u>
	Internal Examiner	Signature	Date
3.	<u>Dr. Rabiul Hussain</u>		<u>12 / July / 2021</u>
	Chairman of Examiner	Signature	Date
4.	<u>Dr. Paulos Taddesse</u>		<u>12 / July / 2021</u>
	Main Advisor	Signature	Date
5.	<u>Dr. Olu femi</u>		<u>12 / July / 2021</u>
	Co- Advisor	Signature	Date

## ACKNOWLEDGEMENT

First and foremost, I would like to praise and thank God, the almighty, for his blessings, knowledge, strength to accomplish this thesis and for everything he has done for me.

My heart felt gratitude goes to my principal advisor Dr. Paulos Tadesse who expertly guided me through my research work and also I would like to thank him for his support, empathy, suggestion, instruction have served the major contributor towards the completion of this research work.

I would like to express my sincere gratitude to my co- advisor Dr. Olu Emmanuel Femi for his continuous support, guidance and encouragement.

My sincere gratitude also goes to Mohammed Hussein MSc. for his benevolence, support and patience.

This work wouldn't have been possible without the financial support of Jimma University to complete this work and also I would like to thank Jimma University Institute of technology for giving me the scholarship.

I am thankful to Dr. N. Murali, Andhra university, India for his support during the VSM, UV-Vis, FE-SEM characterization and also my appreciation goes to the faculty of material science and engineering, Arbaminch University department of physics and chemistry, Adama university and Addis Ababa University for their help during this research work by providing the characterization facilities.

Most importantly I am extremely grateful to my family for their love, support, prayers, caring, guidance and sacrifices for educating me and preparing me for my future and I am also grateful to all of those with whom I have had the pleasure to work during this research work.

My special thanks goes to Dr. Yosef Bekele (Yoye) for his encouragement and endless support.

## ABSTRACT

*Ni<sub>0.6</sub>Zn<sub>0.4-x</sub>Mg<sub>x</sub>Fe<sub>2</sub>O<sub>4</sub> (x = 0.0, 0.1, 0.15, and 0.2) nanoferrites were successfully synthesized by the sol-gel combustion method. The structural, optical and magnetic properties of these materials were investigated using x-ray powder diffraction (XRD), field emission scanning electron microscopy (FE-SEM), Fourier transform infrared (FT-IR) spectroscopy, ultraviolet visible (UV-Vis) spectroscopy, and vibration sample magnetometer (VSM). From the XRD analysis, the lattice parameters and the unit cell volumes of the synthesized samples decreased with an increase in Mg content up to x = 0.15, after which it was increased with a further addition of Mg content (x = 0.2). The crystallite sizes were found between 47.5 and 71.5 nm, indicating that all the synthesized materials possessed a nanocrystalline structure. The FE-SEM micrographs confirmed that all samples have nearly spherical shaped grains with some agglomeration. From FT-IR measurements, the higher frequency bands  $\nu_1$  were appeared between 583.0 and 596.2  $\text{cm}^{-1}$ , and the lower frequency bands  $\nu_2$  were also appeared between 429.7 and 476.7  $\text{cm}^{-1}$ . These bands revealed the presence of the stretching vibration of the metal-oxygen ions at the tetrahedral and octahedral sites. From the optical property study, it was identified that all the synthesized samples were optically activated under ultraviolet light. The optical band gap energies were found between 1.7 and 1.83 eV. The magnetic property study confirmed the soft magnetization behavior of the synthesized samples at room temperature. The squareness ratio values of all samples were found to be less than 0.5, indicating the formation of multi-domain grains.*

**Keywords:** *magnesium substitution, nano-ferrites, sol–gel combustion*

## TABLE OF CONTENTS

DECLARATION .....	i
ACKNOWLEDGEMENT .....	iii
<i>ABSTRACT</i> .....	iv
TABLE OF CONTENTS.....	v
LIST OF TABLES.....	vii
LIST OF FIGURES .....	viii
LIST OF ABBREVIATIONS.....	ix
CHAPTER ONE .....	1
INTRODUCTION .....	1
1.1. Background .....	1
1.2. Statement of the Problem .....	2
1.3. Objective of the study .....	3
1.3.1. General Objective .....	3
1.3.2. Specific Objectives .....	3
1.4. Scope .....	3
1.5. Significance of the Study .....	4
CHAPTER TWO .....	5
LITERATURE REVIEW .....	5
2.1. Ferrites.....	5
2.1.1. Classification of ferrites.....	6
2.1.1.1. Soft ferrites .....	6
2.1.1.2. Hard ferrites .....	7
2.2. Spinel ferrites .....	9
2.3. Types of spinel ferrites.....	10
2.3.1. Normal spinel ferrites .....	10
2.3.2. Inverse spinel ferrites .....	11
2.3.3. Mixed spinel ferrites .....	11
2.4. Nickel ferrite .....	12

2.5. Literature survey .....	13
CHAPTER THREE .....	17
MATERIAL AND METHODS .....	17
3.1 List of chemicals .....	17
3.2 Experimental procedures.....	18
3.2.1 Sample preparation .....	18
3.3 Material characterization.....	20
3.3.1 X-Ray power diffraction .....	20
3.3.2 Field emission scanning electron microscope.....	21
3.3.3 Fourier transform infrared spectroscopy.....	21
3.3.4 Ultraviolet–visible spectroscopy.....	22
3.3.5 Vibrating sample magnetometer .....	23
CHAPTER FOUR.....	24
RESULT AND DISSCUTION.....	24
CHAPTER FIVE .....	35
CONCLUSION AND RECOMMENDATION.....	35
5.1. Conclusion.....	35
5.2. Recommendation .....	36
REFERENCES .....	37



## LIST OF TABLES

Table 2.1. Classification of ferrites.....	10
Table2.2. Category of spinel structure.....	12
Table3.1. List of chemicals, their formula and purpose. ....	17
Table 4.1: Structural parameters for $\text{Ni}_{0.6}\text{Zn}_{0.4-x}\text{Mg}_x\text{Fe}_2\text{O}_4$ nanoparticles.....	26
Table 4.2: Tetrahedral (v1) and octahedral (v2) absorption bands of $\text{Ni}_{0.6}\text{Zn}_{0.4-x}\text{Mg}_x\text{Fe}_2\text{O}_4$ nanoparticles.....	29
Table 4.3: Saturation magnetization (Ms), remanent magnetization(mr), coercivity (Hc), and squareness ratio (Mr/Ms) of all samples.....	34

## LIST OF FIGURES

Figure 2.1: Hysteresis loop for (a) soft and (b) hard ferrite.....	8
Figure 2.2: Schematic of a representative spinel ferrite structure showing oxygen atoms (red) tetrahedral (yellow) and octahedral (green) units.....	9
Figure 2.3. Unit cell structure of (a) normal spinel ferrite, and (b) inverse spinel ferrite. ....	11
Figure 3.1. Schematic diagram for the preparation of $\text{Ni}_{0.6}\text{Zn}_{0.4-x}\text{Mg}_x\text{Fe}_2\text{O}_4$ ( $X= 0.0, 0.1, 0.15, 0.2$ ) nanoferrites by sol-gel combustion method. ....	19
Figure 4.1: XRD patterns for $\text{Ni}_{0.6}\text{Zn}_{0.4-x}\text{Mg}_x\text{Fe}_2\text{O}_4$ nanoparticles. ....	25
Figure 4.2: Shifting of the (311) XRD peaks for $\text{Ni}_{0.6}\text{Zn}_{0.4-x}\text{Mg}_x\text{Fe}_2\text{O}_4$ nanoparticles.....	25
Figure 4.3. FE-SEM images for $\text{Ni}_{0.6}\text{Zn}_{0.4-x}\text{Mg}_x\text{Fe}_2\text{O}_4$ nanoferrites. ....	27
Figure 4.4: FT-IR spectra for $\text{Ni}_{0.6}\text{Zn}_{0.4-x}\text{Mg}_x\text{Fe}_2\text{O}_4$ nanoparticles. ....	28
Figure 4.5: UV–Vis absorbance spectra for $\text{Ni}_{0.6}\text{Zn}_{0.4-x}\text{Mg}_x\text{Fe}_2\text{O}_4$ nanoparticles.....	30
Figure 4.6: Tauc plots for $\text{Ni}_{0.6}\text{Zn}_{0.4-x}\text{Mg}_x\text{Fe}_2\text{O}_4$ nanoparticles.....	31
Figure 4.7: Hysteresis curves for $\text{Ni}_{0.6}\text{Zn}_{0.4-x}\text{Mg}_x\text{Fe}_2\text{O}_4$ nanoparticles.....	33
Figure 4.8: The Magnified view of hysteresis loops of $\text{Ni}_{0.6}\text{Zn}_{0.4-x}\text{Mg}_x\text{Fe}_2\text{O}_4$ nanoparticles.....	34

## **LIST OF ABBREVIATIONS**

FE-SEM	Field Emission Scanning Electron Microscopy
FT-IR	Fourier Transform Infrared
Mr	Remanent Magnetization
Ms	Saturation Magnetization
UV-Vis	Ultraviolet-Visible
VSM	Vibrating Sample Magnetometer
XRD	X-Ray Powder Diffraction

# CHAPTER ONE

## INTRODUCTION

### 1.1. Background

Magnetic properties of nanometer sized particles have attracted considerable attention in recent years because of their unique electrical and magnetic properties due to both, surface and quantum effects, nano-material are considerably different from their bulk form. Therefore, this effect affects extensively the physical properties of these materials specially electrical, magnetic and optical ones. Magnetic nano particles have become more and more important for applications ranging from biotechnology and materials science to biomedicine, as well as technical ones like magnetic data storage over the past few years [1]. For instance, it is worth mentioning the wide range applicability of nano-crystalline nickel zinc magnetic particles have drawn considerable attention of researchers due to their wide range of potential applications such as high-density information storage devices, microwave devices, transformer cores, NEM/MEMs, magnetic fluids, etc. As we have mentioned earlier, the surface to volume ratio of these nano magnetic materials is very large as compared to the bulk due to which they exhibit unique properties such as spin canting, surface anisotropy, super paramagnetism, etc. [2].

Magnetite and spinel ferrite nanocrystals are regarded as two of the most important inorganic nano material because of their electronic, optical, electrical, magnetic, and catalytic properties, all of which are different from the properties of their bulk counterparts. Among the spinel ferrites compounds, zinc ferrite, magnesium ferrite, and cadmium ferrite have been studied extensively due to their different structures composed of inverse, normal, and mixed spinel structures, respectively, and their high electromagnetic performance, excellent chemical stability, mechanical hardness, low coercivity and moderate saturation magnetization, which make it a good contender for the application as soft magnets and low-loss materials at high frequencies.

The physical properties of nanoparticles are of current interest due to the size-dependent behavior observed in the nanometer length scale and high crystallinity. Nickel and zinc are known to have strong preference for the tetrahedral and octahedral sites, respectively, making nickel ferrite a model inverse ferrite and zinc ferrite a model normal ferrite. However, the composite Ni–Zn ferrites are known to exist as mixed spinel structure [3].

The compositional variation in these ferrites results in the redistribution of metal ions over the tetrahedral and octahedral sites, which can modify the properties of ferrites. It is also known that the physical properties of the ferrites are very sensitive to the method of synthesis and the type of substitution. The selection of an appropriate process is, therefore, the key to obtain good quality ferrites. Various synthesis processes have been used for preparing nano sized ferrite particles. These include sol-gel, hydrothermal, chemical co precipitation, sono-chemical reactions, mechanical ball milling, etc. of all these processes, sol gel combustion method is the most convenient method for the synthesis of nano particles as it produces high purity and uniform nanostructures at low temperature [4]. On the other hand the magnetic properties of these oxides depend on the type of cations and their distribution among the two interstitial positions. The cation distribution and the resulting magnetic properties are found to be different and quite interesting in some nano-crystalline spinel ferrites when compared to those of their bulk counterparts [5].

In this research, we studied the effect of Mg substitution on the structural, optical and magnetic properties of  $\text{Ni}_{0.6}\text{Zn}_{0.4-x}\text{Mg}_x\text{Fe}_2\text{O}_4$  nanoferrite with x varying from 0 to 0.2 prepared by sol-gel combustion method. X-ray powder diffraction (XRD), Field emission scanning electron microscopy (FE-SEM), Fourier transform infrared (FT-IR) spectroscopy, ultraviolet visible (UV-Vis) spectroscopy and vibration sample magnetometer (VSM) characterizations were used to investigate the desired properties.

## **1.2. Statement of the Problem**

The growing demand for electronic devices for application in almost all fields leads to the use of nano materials due to their unique property compared to the bulk ones that arise from the surface area to volume ratio difference. Nano magnetic materials are a class of nano sized materials having an outstanding electromagnetic property. Many works have been done on Ni-Zn nanoferrite, and that the structural, optical and magnetic properties of these nano materials depend on the size of the particles, the substitution and the type of synthesis methods [6,7]. From the literature survey, it is also identified that by the introduction of a relatively small amount of foreign metallic ions into spinel materials, important modification in structure, optical as well as magnetic properties can be obtained.

In view of the significant importance of Ni-Zn based nano sized ferrites and the fact that their properties undergo significant changes on substitution with metal cations as well as the synthesis method, in this work the structural, optical and magnetic properties of Mg substituted  $\text{Ni}_{0.6}\text{Zn}_{0.4-x}\text{Mg}_x\text{Fe}_2\text{O}_4$  ( $x = 0.1, 0.15, 0.2$ ) nanoferrite synthesized by using sol-gel combustion technique were studied. From an intensive literature survey, it was identified that no reports have been cited on the optical and magnetic property of  $\text{Ni}_{0.6}\text{Zn}_{0.4}\text{Fe}_2\text{O}_4$ ,  $\text{Ni}_{0.6}\text{Zn}_{0.3}\text{Mg}_{0.1}\text{Fe}_2\text{O}_4$ ,  $\text{Ni}_{0.6}\text{Zn}_{0.25}\text{Mg}_{0.15}\text{Fe}_2\text{O}_4$  and  $\text{Ni}_{0.6}\text{Zn}_{0.2}\text{Mg}_{0.2}\text{Fe}_2\text{O}_4$  nanoparticles synthesized by sol-gel combustion technique.

### **1.3. Objective of the study**

#### **1.3.1. General Objective**

The general objective of this study is to investigate the effect of magnesium substitution on the structural, optical and magnetic properties of nickel-zinc nanoferrite prepared by sol-gel combustion method.

#### **1.3.2. Specific Objectives**

- To synthesize  $\text{Ni}_{0.6}\text{Zn}_{0.4-x}\text{Mg}_x\text{Fe}_2\text{O}_4$  ( $x = 0.0, 0.1, 0.15, 0.2$ ) nanoferrites by using sol-gel combustion method.
- To characterize the prepared samples using XRD, FE-SEM, FT-IR spectroscopy, UV-Vis spectroscopy, and VSM.
- To compute different structural parameters, such as lattice constants, unit cell volumes, crystallite sizes, and magnetic parameters, such as the saturation magnetization, coercivity, and retentivity of the synthesized samples.

### **1.4. Scope**

This research work encompasses the formation of magnesium substituted Ni-Zn nanoferrite using sol-gel combustion technique and investigation of the different properties including structural, optical and magnetic property of the synthesized nanoparticle using various characterization methods.

### **1.5. Significance of the Study**

It is concluded that the physical properties such as electrical, optical, structural and magnetic properties of material are mostly depend on the size of the particle and the synthesis technique. In the present work the structural, optical and magnetic properties of  $\text{Ni}_{0.6}\text{Zn}_{0.4-x}\text{Mg}_x\text{Fe}_2\text{O}_4$  x varying from 0.0 to 0.2 in a nano-level synthesized using sol-gel combustion method was investigated. Why we preferred sol-gel combustion method is due to its various advantages like better homogeneity, composition control, simple, narrow particle size distribution at relatively low temperature as it is a wet chemical method, high purity compared to other methods. The characterization techniques that have been employed in order to study the required properties like structural, optical and magnetic after substitution of magnesium in the parent material are XRD, FE-SEM, FT-IR spectroscopy, UV-Vis spectroscopy, and VSM. Owing to this an outstanding result has been obtained on the corresponding material.

The findings of this research will be a significant endeavor for beginner researchers on the field of nanomagnetic materials and will give contribution through giving information about nanoparticles and synthesis technique. It also serves as a future reference for researchers on this area. Therefore, this work will be helpful on giving information about the different properties of the prepared sample materials in detail.

## CHAPTER TWO

### LITRATURE REVIEW

#### 2.1. Ferrites

Ferrite is a general term used for any ferrimagnetic ceramic material. They are a very well established group of magnetic materials. Various types of ferrites are commercially important. Ferrite is categorized as electro ceramics with ferrimagnetic properties. Each one has a unique crystal structure, magnetic, electric and dielectric properties. Ferrites or ferromagnetic oxides (also known as ceramics containing compounds of iron) are dark brown or gray in appearance and very hard and brittle in physical character. They are prepared by heat-treating various transition metal oxides or alkaline earth oxides with the ferric oxides. The magnetic behavior exhibited by the ferrites is quite different from ferromagnetism that is exhibited by metallic materials. Ferrites are non-conducting magnetic media so eddy current and ohmic losses are less than for ferromagnetic materials. Ferrites are often used as transformer cores at radio frequencies (RF), simple permanent magnets, and magnetic recording. These applications are based upon the very basic properties of ferrites: a significant saturation magnetization, a high electrical resistivity, low electrical losses, and a very good chemical stability, ferrites are most common in nature. From the daily iron oxide  $\text{Fe}_3\text{O}_4$  (magnetite) formed at the surface of many iron containing objects like fences, cars, doors, barbecue grills.

Ferrite exhibits ferrimagnetism due to the super-exchange interaction between electrons of metal and oxygen ions. The opposite spins in ferrite results in the lowering of magnetization compared to ferromagnetic metals where the spins are parallel. Due to the intrinsic atomic level interaction between oxygen and metal ions, ferrite has higher resistivity compared to ferromagnetic metals. This enables the ferrite to find applications at higher frequencies and makes it technologically very valuable. Their magnetic properties can greatly vary from one element to another, since the microscopic (atomic) structure is composed of two or more magnetic sublattices.



Many ferrites are spinels with the formula  $AB_2O_4$ , where A and B represent various metal cations, usually including iron (Fe). Spinel ferrites usually adopt a crystal motif consisting of cubic close-packed (FCC) oxides ( $O_2^-$ ) with A cations occupying one eighth of the tetrahedral holes and B cations occupying half of the octahedral holes.

If one eighth of the tetrahedral holes are occupied by B cation, then one fourth of the octahedral sites are occupied by A cation and the other one fourth by B cation and it's called the inverse spinel structure. It's also possible to have mixed structure spinel ferrites with formula  $[M^{2+}_{1-\delta}Fe^{3+\delta}][M^{2+\delta}Fe^{3+2-\delta}]O_4$  where  $\delta$  is the degree of inversion [8]. The magnetic material known as "ZnFe" has the formula  $ZnFe_2O_4$  with  $Fe^{3+}$  occupying the octahedral sites and  $Zn^{2+}$  occupy the tetrahedral sites [9]. The possibility of preparing ferrites in the form of nanoparticles has opened a new and exciting research field, with revolutionary applications not only in the electronic technology but also in the field of biotechnology [5].

### **2.1.1. Classification of ferrites**

Ferrites are classified according to magnetic properties and their crystal structure. Based on their magnetic properties, ferrites are often classified as "soft" and "hard" which refers to their low or high coercivity of their magnetism, respectively.

#### **2.1.1.1. Soft ferrites**

Soft ferrites are characterized by a small value of coercivity so they cause low hysteresis loss at high frequency owing to which they are widely used in electromagnetic cores of transformers, switching circuits in computers and RF inductors; e.g., lithium ferrite, nickel ferrite and manganese-zinc ferrite [10]. Soft ferrites are ferrimagnetic materials with cubic crystal structure and they are characterized by a chemical formula  $MO \cdot Fe_2O_3$ , where M is transition metal ions like Iron, Nickel, Manganese or Zinc. Manganese-Zinc ferrites are used in soft magnetic applications up to high frequencies of 10 MHz. At high frequency, metallic soft magnetic materials simply cannot be used due to the eddy current losses. Therefore, soft ferrites, which are ceramic insulators, become the most desirable material for example in telephone signal transmitters and receivers and in switch mode power supplies (referred as DC-DC converters).

Ferrites that are used in transformer or electromagnetic cores contain nickel, zinc, or manganese compounds. They have a low coercivity and are called soft ferrites. Due to their comparatively low losses at high frequencies, they are extensively used in the cores of switched mode power supply (SMPS) and radio-frequency (RF) transformers and inductors.

#### **2.1.1.2. Hard ferrites**

Hard ferrites are characterized by a large value of retentivity and coercivity after magnetization so they find applications as permanent magnets in radios; e.g., barium and strontium ferrite. Maximum magnetic field strength is about 0.35 T and magnetic field strength is about 30 to 160 kA/m. Permanent ferrite magnets are made up of hard ferrites, which have a high coercivity and high remanence after magnetization. These ferrites are composed of iron and barium or strontium oxides. In a magnetically saturated state they conduct magnetic flux well and have a high magnetic permeability. This enables these ceramic magnets to store stronger magnetic fields than iron itself. They are cheap, and are widely used in household products such as refrigerator magnets. The hexagonal ferrite structure is found in both  $Ba_{0.6}Fe_2O_3$  and  $Sr_{0.6}Fe_2O_3$ , but Sr-M hexaferrite has slightly superior magnetic properties.

In contrast, permanent ferrite magnets (or hard ferrites) which have a high remanence after magnetization are composed of iron and barium or strontium oxides. In a magnetically saturated state, they conduct magnetic flux well and have a high magnetic permeability. This enables these so-called ceramic magnets to store stronger magnetic fields than iron itself. They are the most commonly used magnets in radios. The maximum magnetic field  $B$  is about 0.35 Tesla and the magnetic field strength  $H$  is about 30 to 160 kA turns per meter (400–2,000 Oe) [11].

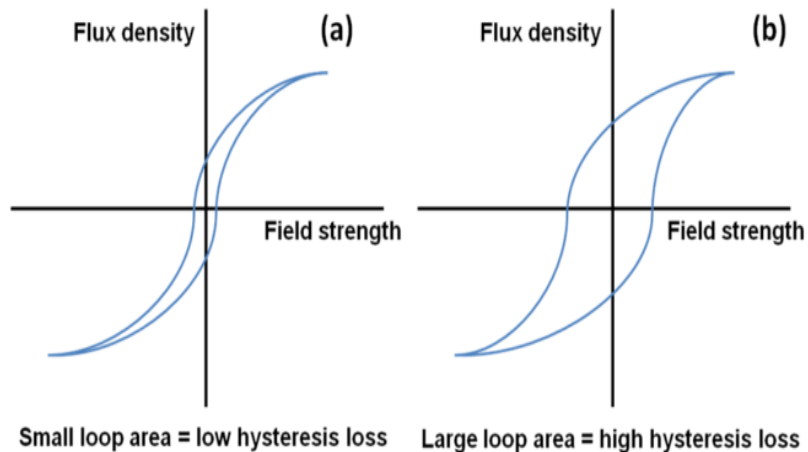


Figure 2.1: Hysteresis loop for (a) soft and (b) hard ferrite.

Ferrites can also be classified into the following three different type;

1. Hexagonal ferrite
2. Garnet
3. Ortho ferrite
4. Spinel ferrite (Cubic ferrite)

### Hexagonal ferrites

Hexagonal ferrites was first identified by Went *et al.* in 1952 [12] and Jonker *et al.* in 1956. These types of ferrites have a formula  $MFe_{12}O_{19}$ , where M is an element like Barium, Lead or Strontium. In these ferrites, oxygen ions have closed packed hexagonal crystal structure. They are widely used as permanent magnets and have high coercivity. They are used at very high frequency. Their hexagonal ferrite lattice is similar to the spinel structure with closely packed oxygen ions, but there are also metal ions at some layers with the same ionic radii as that of oxygen ions. Hexagonal ferrites have larger ions than that of garnet ferrite and are formed by the replacement of oxygen ions. Most of these larger ions are barium, strontium or lead [13].

### Garnets

The general formula of the unit cell of a pure iron garnet has eight formula units of  $M_3Fe_5O_{12}$ , where M is the trivalent rare earth ions (Y, Gd, Dy). Their cell shape is cubic and the edge length is about 12.5 Å. They have complex crystal structure. They are largely used in applications of memory structure [13].

## Ortho Ferrites

Ortho-ferrites have an ortho-rhombic crystal structure and space group Pbnm. The chemical formula of these ferrites is,  $RFeO_3$  where R is the rare-earth element. Ortho-ferrites are commonly weak ferromagnetic materials  $LaFeO_3$  and  $DyFeO_3$  are examples of ortho-ferrites [14]. Ortho ferrites possess extremely high velocities of the domain wall motion and it is used in communication techniques, in optical internet, in sensors of magnetic fields and electrical currents, mechanical quantities etc. [8]

## 2.2 Spinel ferrites

Ferrites with the formula  $AB_2O_4$ , constitute the first group of ferrites, where A and B represent various metal cations like iron. The crystal structure spinel ferrite is cubic with spinel type ( $MgAl_2O_4$ ) and possesses two tetrahedral and four octahedral sites per unit formula. The unit cell of spinel ferrites is FCC with eight formula units per unit cell. The formula can be written as  $M_8Fe_{16}O_{32}$ . The anions are the greatest and they form an FCC lattice. Within these lattices two types of interstitial positions occur and these are occupied by the metallic cations. There are 96 interstitial sites in the unit cell, 64 tetrahedral (A) and 32 octahedral (B) sites.

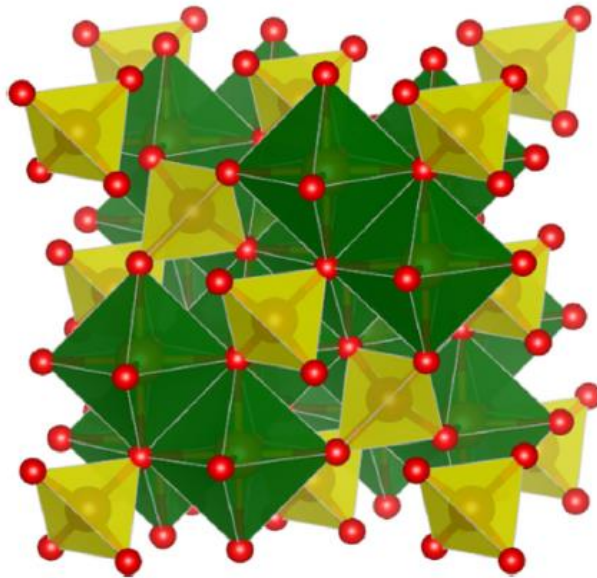


Figure 2.2. Schematic of a representative spinel ferrite structure showing oxygen atoms (red) tetrahedral (yellow) and octahedral (green) units [15].

Ions located at the tetrahedral sites are known as ‘network formers’, while those located at the octahedral sites are known as ‘network modifiers’ [16]. Such a structure endows the spinel ferrites with unique electromagnetic properties [17-18].

Spinel ferrites are magnetically soft and they are alternative to metallic magnets such as Fe and layered Fe-Si alloys, but exhibit enhanced performance due to their outstanding magnetic properties. In addition, spinel ferrites have the properties such as high electrical resistivity and low magnetic loss.

The two popular ceramic magnets; Nickel-Zinc ferrites and Manganese-Zinc ferrites are the major members of the spinel ferrite family. They have been intriguing ceramic materials due to their high electrical resistivity, high magnetic permeability and possible modification of intrinsic properties over a wide spectrum [4].

Table 2.1. Classification of ferrites [8].

Types	Molar ratio	Representations
Spinel	$\text{Fe}_2\text{O}_3 \cdot 1\text{MO}$	MO is a transition metal oxide
Garnet	$5\text{Fe}_2\text{O}_3 \cdot 3\text{M}_2\text{O}_3$	$\text{M}_2\text{O}_3$ is a rare earth metal oxide
Ortho	$\text{AFeO}_3$	A is rare earth elements like HO, Dy, Er, Y, Yb
Hexaferrite	$6\text{Fe}_2\text{O}_3 \cdot 1\text{MO}$	MO is a divalent metal oxide from group IIA e.g. BaO, CaO, SrO

## 2.2. Types of spinel ferrites

Based on their crystal structure spinel ferrites are classified into three different groups namely; normal spinel ferrites, inverse spinel ferrites and mixed spinel ferrites.

### 2.2.1. Normal spinel ferrites

If there is only one kind of cations on octahedral (B) sites, the spinel is normal. In these ferrites the divalent cations occupy tetrahedral (A) sites, while the trivalent cations are on octahedral (B) sites[19]. The cation distribution for normal spinel ferrites can be represented as in general  $(\text{A}^{2+})^{\text{A}}[\text{B}^{3+}_2]^{\text{B}}\text{O}_4$ .

Some examples of normal spinel ferrites are zinc ferrite ( $\text{ZnFe}_2\text{O}_4$ ) and cadmium ferrites ( $\text{CdFe}_2\text{O}_4$ ), in which the divalent metallic ions  $\text{Zn}^{2+}$  or  $\text{Cd}^{2+}$  are at the (A) site, while  $\text{Fe}^{3+}$  ions are at (B) site. Their structures are usually cubic close-packed oxides with eight tetrahedral and four octahedral sites per formula unit. The tetrahedral spaces are smaller than the octahedral spaces. B ions occupy half the octahedral holes, while A ions occupy one-eighth of the tetrahedral holes [20].

### 2.2.2. Inverse spinel ferrites

In inverse spinel structure, half of the  $\text{Fe}^{3+}$  ions occupy A-sites and remaining occupy B-sites and its general formula can be written as  $([\text{M}^{2+} \text{Fe}^{3+}]^{\text{B}} [\text{Fe}^{3+}]^{\text{A}} \text{O}_4)$  (e.g.,  $\text{FeOFe}_2\text{O}_3$ ,  $\text{NiFe}_2\text{O}_4$ ,  $\text{CoFe}_2\text{O}_4$ ). For an inverse spinel, all the divalent metal ions  $\text{A}^{2+}$  are located at octahedral B sites and trivalent ions  $\text{B}^{3+}$  are distributed equally between the A and B sites[8].

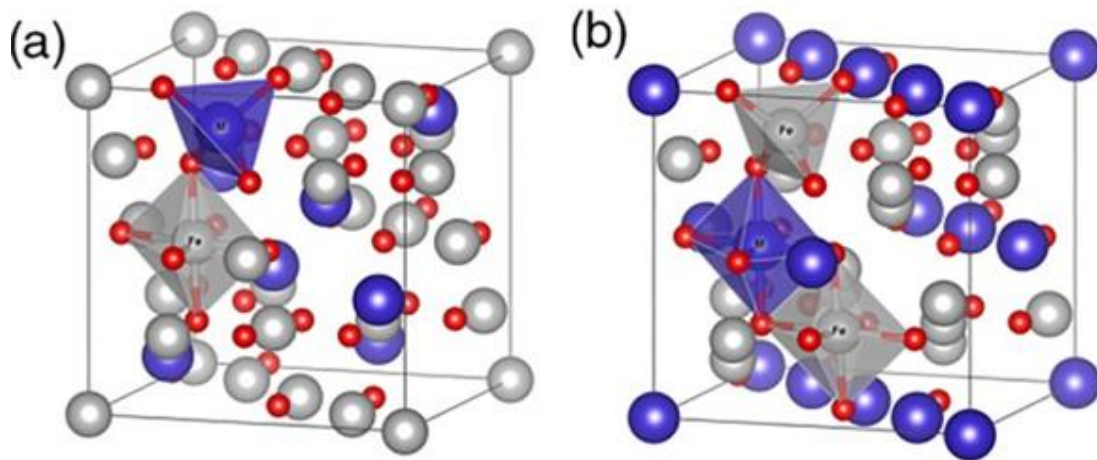


Figure 2.3. Unit cell structure of (a) normal spinel ferrite, and (b) inverse spinel ferrite [21].

### 2.2.3. Mixed spinel ferrites

In this type of ferrites, the divalent metal ions  $\text{A}^{2+}$  and trivalent  $\text{B}^{3+}$  ions are distributed at both tetrahedral A site and octahedral B site then the ferrite is termed as random spinel ferrite. Iron based random spinel ferrites can be represented by  $[\text{M}_x^{2+} \text{Fe}_{1-x}^{3+}]^{\text{A}} [\text{M}_{1-x}^{2+} \text{Fe}_{1+x}^{3+}]^{\text{B}} \text{O}_4$ , where  $x$  is inversion parameter, depends on the method of preparation of ferrite and chemical composition of ferrite. For complete normal spinel ferrite  $x = 1$ , for

complete inverse spinel ferrite  $x = 0$ , for mixed ferrite 'x' ranges between these two extreme values, for completely mixed ferrite  $x = 1/3$ . Examples for mixed spinel ferrite are  $MnFe_2O_4$ ,  $MgFe_2O_4$  [22].

**Table 2.2. Category of spinel structure [8].**

Structure	Chemical formula	Sites	
		Tetrahedral	Octahedral
Normal spinel	$(A^{2+})[B^{3+}]_2O_4^{2-}$	All $A^{2+}$ cations occupy	$B^{2+}$ cations occupy
Invers spinel	$(B^{3+})[A^{2+}B^{3+}]O_4^{2-}$	$1/2B^{3+}$ cations occupy	$1/2B^{3+}$ and all $A^{2+}$ cations occupy
Mixed spinel	$(A_{1-\delta}^{2+}B_{\delta}^{3+})\left[A_{\frac{\delta}{2}}^{2+}B_{1-\frac{\delta}{2}}^{3+}\right]$	<ol style="list-style-type: none"> <li><math>0 &lt; \delta &lt; 1</math></li> <li>If <math>\delta = 0</math> the normal spinel and if <math>\delta = 1</math> the inverse spinel. So <math>\delta</math> can be referred to as tenable factor between normal, inverse and mixed structures.</li> </ol>	

### 2.3. Nickel ferrite

Nickel ferrite with the formula  $NiFe_2O_4$  has an inverse spinel structure; i.e. oxygen ions have cubic closed packing arrangement. Out of the total 64 tetrahedral sites (A sites), 8 are occupied by  $Fe^{3+}$ , 8  $Ni^{2+}$  and 8  $Fe^{3+}$  are occupied in 16 octahedral sites (B sites) of a possible 32 [23]. There is anti-ferromagnetic coupling between the A and B atoms and a net magnetic moment is obtained due to the nickel ions.  $Ni^{2+}$  has a magnetic moment of  $2 \mu_B$  and hence a unit cell of the ferrite has a total magnetic moment of  $16 \mu_B$ .

$NiFe_2O_4$  nanoparticles have been widely studied for their unique properties which can be influenced by their shape, particle size and their composites with other material and have different applications [24]. Due to their high electric resistivity, low coercivity, moderate saturation magnetization and low hysteresis losses, nickel ferrites are categorized in the class of soft ferrites [25-26]. These soft magnetic materials also offer other favorable properties, such as high permeability at high frequency, mechanical hardness, electrochemical stability, reasonable cost and low dielectric and eddy current losses [12, 27].

Various methods are used to synthesize Nickel ferrite nanoparticles, such as: combustion, redox process, forced hydrolysis, co-precipitation, sol-gel, hydrothermal, polymer combustion method (PC), solid state method (SS), electrochemical, thermal decomposition method and sol-gel auto combustion method [28-31].

#### **2.4. Literature survey**

In recent years, a lot of work has been done on nanomagnetic materials because of their unique properties compared to the bulk materials. Many researchers are involved in the investigations of Ni-Zn based nanoparticles because of their potential applications in almost all electromagnetic devices, microwave technology and high-density magnetic recording media, biomedicine etc. Some of them are discussed as follows.

Jagadeesh Kumar et al. [1] have investigated the Copper-substituted Ni-Zn nanoferrite prepared by using sol-gel technique using polyvinyl alcohol as a chelating agent to control the particle size. The structural parameters and magnetic properties were examined by X-ray diffraction, field emission scanning electron microscopy (FESEM), Fourier-transform infrared spectroscopy and vibrating-sample magnetometer techniques respectively. They identified that the substitution of Cu affects the structural and the physical properties of Ni-Zn nanoferrite. The observed high values of magnetic permeability and DC resistivity suggest that the Ni-Zn ferrite system yields useful electromagnetic properties for smaller concentrations of copper substitution.

Kandasamy Velmurugan et al. [3] have reported nickel ferrite of sizes 6 to 8 nm nanoparticles synthesized by using co-precipitation method with  $x$  varying from 0 to 1.0. The powder samples were characterized by XRD, VSM and FTIR. The average crystallite sizes of the particles were determined from X-ray diffraction. X-ray analysis showed that the samples were cubic spinel. The lattice constant ( $a$ ) increased with an increase in zinc content. The specific saturation magnetization ( $M_s$ ) of the particles was measured at room temperature. The magnetic parameter of  $M_s$  was found to decrease with the increase in zinc substitution. Fourier transform infrared spectroscopy (FTIR) spectra of the  $Ni_{1-x}Zn_xFe_2O_4$  with  $x = 0, 0.5, 1$  in the range  $400 - 4000\text{ cm}^{-1}$  were reported. The spinel structure and the crystalline water adsorption of  $Ni_{1-x}Zn_xFe_2O_4$  nanoparticles were studied by using FTIR.



Bobade et al. [32] studied nanocrystalline arrays of Ni<sup>2+</sup> substituted Mg–Zn spinel ferrite having a generic formula Mg<sub>0.7x</sub>Ni<sub>x</sub>Zn<sub>0.3</sub> Fe<sub>2</sub>O<sub>4</sub> (x=0.0, 0.2, 0.4 and 0.6) which were successfully synthesized by sol–gel auto-combustion technique. The fuel used in the synthesis process was citric acid and the metal nitrate-to-citric acid ratio was taken as 1:3. The phase, crystal structure and morphology of Mg–Ni–Zn ferrites were investigated by X-ray diffraction, scanning electron microscopy, and Fourier transformer infrared spectroscopy techniques. The lattice constant, crystallite size, porosity and cation distribution were determined from the X-ray diffraction data method. The FTIR spectroscopy is used to deduce the structural investigation and redistribution of cations between octahedral and tetrahedral sites of Mg–Ni–Zn spinel structured material. Morphological investigation suggests that the formation of grain growth as the Ni<sup>2+</sup> content x increases. The saturation magnetization and magneton number were determined from hysteresis loop technique. The saturation magnetization increases with increasing Ni<sup>2+</sup> concentration 'x' in Mg–Zn ferrite.

Sareh Shafiee et al. [33] reported the Zinc, magnesium, and copper substituted nickel spinel ferrite which were synthesized in the form of Ni<sub>1-x</sub>(Zn<sub>0.6</sub>Mg<sub>0.2</sub>Cu<sub>0.2</sub>)<sub>x</sub> Fe<sub>2</sub>O<sub>4</sub> (where x = 0.0, 0.3, 0.5 and 0.7) via auto combustion method. The effect of the presence of these dopants on the average of crystallite, average particle size, the lattice constant, morphology, initial permeability, and magnetization of the synthesized ferrites was investigated. The structural properties, morphology, and magnetic properties were characterized via X-ray diffraction (XRD), field emission scanning electron microscopy (FE-SEM), energy dispersive spectroscopy (EDS), LCR meter and alternative gradient force magnetometer (AGFM). XRD study shows the formation of a single-phase cubic spinel structure. Also, the average crystallite size was found to increase from 6 nm to 11 nm with increasing the Zn<sup>2+</sup>, Mg<sup>2+</sup>, and Cu<sup>2+</sup> doping ratio from 0.0 to 0.7. Moreover, FE-SEM results were indicated the presence of nanosized spherical shape of prepared particles with agglomeration. The lattice constant and the particle size were found to increase with the increase in Zinc, magnesium, and copper. The values of initial permeability and magnetization were increased to a maximum value of 76 H/M and 71.37 emu/g for x = 0.7 sample. Furthermore, coercivity was found to decrease with increasing Zinc, magnesium, and copper concentration, which is useful for power applications. The variations of initial permeability and magnetization as a function of average particle size were discussed and were compared with previous works.

The results were indicated the increase in initial permeability and magnetization with the enhancement of average particle size. The constancy in permeability throughout the frequency range studied from 10 kHz to 1 MHz was indicated the compositional stability and quality of the samples. The results were indicated that the ferrites with high initial permeability can be an excellent choice as magnetic cores.

ShimelisAdem et al. [34] reported the structural, optical properties of  $\text{Zn}_{0.85}\text{Ni}_{0.1}\text{Mg}_{0.05}\text{Fe}_2\text{O}_4$  nanoparticles that were synthesized by using a sol-gel combustion method using the raw materials  $\text{Zn}(\text{NO}_3)_2 \cdot 6\text{H}_2\text{O}$ ,  $\text{Ni}(\text{NO}_3)_2 \cdot 6\text{H}_2\text{O}$ ,  $\text{Mg}(\text{NO}_3)_2 \cdot 6\text{H}_2\text{O}$ ,  $\text{Fe}(\text{NO}_3)_3 \cdot 9\text{H}_2\text{O}$  and  $\text{C}_6\text{H}_8\text{O}_7 \cdot \text{H}_2\text{O}$ . The synthesized  $\text{Zn}_{0.85}\text{Ni}_{0.1}\text{Mg}_{0.05}\text{Fe}_2\text{O}_4$  sample was characterized by X-ray powder diffraction (XRD), Fourier transform infrared (FTIR) spectroscopy and ultraviolet-visible (UV-Vis) spectroscopy. Using these techniques, the structure as well as the optical property of the synthesized sample was investigated. The lattice parameter, unit cell volume and band gap of  $\text{Zn}_{0.85}\text{Ni}_{0.1}\text{Mg}_{0.05}\text{Fe}_2\text{O}_4$  sample were also estimated. The XRD analysis confirmed that the synthesized  $\text{Zn}_{0.85}\text{Ni}_{0.1}\text{Mg}_{0.05}\text{Fe}_2\text{O}_4$  sample possessed a single-phase cubic spinel structure with Fd-3m space group. The lattice parameter, the unit cell volume and the average crystal size of  $\text{Zn}_{0.85}\text{Ni}_{0.1}\text{Mg}_{0.05}\text{Fe}_2\text{O}_4$  sample were found to be 0.8342 nm, 580.5 ( $\text{\AA}$ )<sup>3</sup> and 51 nm, respectively. The FT-IR analysis of  $\text{Zn}_{0.85}\text{Ni}_{0.1}\text{Mg}_{0.05}\text{Fe}_2\text{O}_4$  sample confirms the presence of two strong absorption bands  $\nu_1$  and  $\nu_2$  which lie in the expected range of cubic spinel-type ferrite material. It also revealed the presence of the tetrahedral and octahedral sites in  $\text{Zn}_{0.85}\text{Ni}_{0.1}\text{Mg}_{0.05}\text{Fe}_2\text{O}_4$  sample. The optical band gap of the sample was found to be 2.4 eV, indicating the semiconductor behavior of  $\text{Zn}_{0.85}\text{Ni}_{0.1}\text{Mg}_{0.05}\text{Fe}_2\text{O}_4$  sample.

In 2018 Carlos Andrés Palacio Gómez et al. [35] prepared series of Nickel-Zinc ferrite samples by low-energy ball milling with subsequent thermal treatment in air at 1200 °C for 12 h. X-ray Diffraction patterns confirm the formation of the ferrite phases. Lattice parameters were found to increase almost linearly from 8.3366  $\text{\AA}$  to 8.4387  $\text{\AA}$  with the increment of zinc substitution. The oxygen parameters also increased and were found to closely follow an earlier proposed power law equation. The cation-oxygen bond lengths, suggest a gradual tetrahedral expansion and octahedral contraction with increasing Zn content. Additionally, the occupation of  $\text{Zn}^{2+}$  and  $\text{Ni}^{2+}$  ions in all samples has been determined by using the line intensity ratios of diffraction peaks together with a proposed general chemical formula.

From the calculated cation distributions, it was found that the theoretical lattice parameters agree with the experimental ones. By using, the Williamson-Hall method, an average crystallite size of  $\sim 36$  nm was found.

Shannon A. Morrison et al. [36]. Have also studied the Nickel-zinc ferrite nanoparticles ( $\text{Ni}_{0.2}\text{Zn}_{0.44}\text{Fe}_{2.36}\text{O}_4$ ) have been produced at room temperature, without calcination, using a reverse micelle process. Particle size is approximately 7 nm as determined by x-ray powder diffraction and transmission electron microscopy. Saturation magnetization values are lower than anticipated, but are explained by elemental analysis, particle size, and cation occupancy within the spinel lattice. Extended x-ray absorption fine structure analysis suggests that a significant amount of  $\text{Zn}^{2+}$ , which normally occupies tetrahedral sites, actually resides in octahedral coordination in a zinc-enriched outer layer of the particles. This “excess” of diamagnetic Zn can thus contribute to the overall decrease in magnetism. Further, this model can also be used to suggest a formation mechanism in which  $\text{Zn}^{2+}$  is incorporated at a later stage in the particle growth process.

Abbasher M Gismelseed et al [37] have prepared spinel magnesium-zinc ferrites  $\text{Zn}_x\text{Mg}_{1-x}\text{Fe}_2\text{O}_4$  ( $0 < x < 1$ ) by the standard double sintering ceramic method have been investigated using X-ray (XRD) diffraction technique and Mössbauer spectroscopy measurements at 295K and 78K. The crystal structure is found to be single cubic spinel whose lattice parameter ‘a’ increases with increasing Zn content. The Mössbauer spectra of the samples taken at 78 K are found to be magnetically ordered for  $x=0.5$ , paramagnetic for  $x=0.8$  and show very broad patterns for intermediate concentration of  $\text{Zn}^{2+}$ . The variation of the magnetic properties with the Zn concentration has been explained on the basis of the cation distribution driven from the Mössbauer measurements.

Jamadar et al. [38] synthesized series of nanocrystalline  $\text{Ni}_{0.6-x}\text{Zn}_x\text{Cu}_{0.4}\text{Fe}_2\text{O}_4$  ferrites ( $x = 0.0, 0.1, 0.2, 0.3, 0.4$ ) by auto-combustion route. Formation of the spinel phase (without any impurity phase) was confirmed by X-ray diffraction. The lattice parameter of synthesized ferrites was found to linearly increase with increasing  $x$ . The octahedral and tetrahedral vibration modes were studied by Fourier transform IR spectroscopy. SEM images revealed compact agglomeration exhibiting grain growth with an increase in  $x$ . The dependence of saturation magnetization on the mole fraction of zinc was studied

## CHAPTER THREE

### MATERIAL AND METHODS

#### 3.1 List of chemicals

In this research work, sol-gel combustion technique is proposed to synthesize the desired Mg substituted Ni-Zn nanoferrite. Different chemicals were used (Table 3.1) in order to prepare the required four samples based on the predefined composition.

Table 3.1. List of chemicals, their formula and purpose.

No	Chemicals	Chemical Formula	Purpose
1	Nickel(II) Nitrate Hexahydrate	$\text{Ni}(\text{NO}_3)_2 \cdot 6\text{H}_2\text{O}$	Source of Ni cation
2	Zinc(II) Nitrate Hexahydrate	$\text{Zn}(\text{NO}_3)_2 \cdot 6\text{H}_2\text{O}$	Source of Zn cation
3	Magnesium (II) Nitrate Hexahydrate	$\text{Mg}(\text{NO}_3)_2 \cdot 6\text{H}_2\text{O}$	Source of Mg cation
4	Iron (III) Nitrate Nonahydrate	$\text{Fe}(\text{NO}_3)_3 \cdot 9\text{H}_2\text{O}$	Source of Fe cation
5	Citric Acid Monohydrate	$\text{C}_6\text{H}_8\text{O}_7 \cdot \text{H}_2\text{O}$	Chelating agent
6	Ammonia Solution	$\text{NH}_3$ solution	To adjust pH value of the solution
7	Potassium Bromide	KBr	To produce transparent pellet

## 3.2 Experimental procedures

This section describes the sample preparation technique to synthesize the required Mg substituted Ni-Zn nanoferrite in regular steps and also different characterization technique in detail.

### 3.2.1 Sample preparation

$\text{Ni}_{0.6}\text{Zn}_{0.4-x}\text{Mg}_x\text{Fe}_2\text{O}_4$  nanopowder varying  $x$  from 0.0 to 0.2 in regular steps were prepared by sol-gel combustion method by taking high purity precursor salts. The raw materials used for making the required sample materials were namely Nickel(II) Nitrate Hexahydrate ( $\text{Ni}(\text{NO}_3)_2 \cdot 6\text{H}_2\text{O}$ ), Zinc(II) Nitrate Hexahydrate ( $\text{Zn}(\text{NO}_3)_2 \cdot 6\text{H}_2\text{O}$ ), Magnesium (II) Nitrate Hexahydrate ( $\text{Mg}(\text{NO}_3)_2 \cdot 6\text{H}_2\text{O}$ ), Iron (III) Nitrate Nonahydrate ( $\text{Fe}(\text{NO}_3)_3 \cdot 9\text{H}_2\text{O}$ ) and citric acid ( $\text{C}_6\text{H}_8\text{O}_7 \cdot \text{H}_2\text{O}$ ) was used in the reaction as a fuel and chelating agent in order to facilitate a good medium for dispersion of nanoparticles and to control the particle growth during the synthesis process. The weighed amounts of these ingredients were dissolved in minimum amounts of deionized water in stoichiometric ratio, the expected metal nitrate and citric acid were maintained in molar ratio 1:1. And then ammonia solution ( $\text{NH}_4\text{OH}$ ) was added drop wise until PH of 7 was attained under a continuous stirring. Later the prepared solution was then stirred with a magnetic stirrer at about  $100^\circ\text{C}$ . As the evaporation of water proceeded, the sol turned into viscous gel. Then the obtained gel further heated for 3 hours at  $100^\circ\text{C}$  to remove the volatile impurities.

During heating process the gel gets boiled and combustion process carried out in the hottest zones of the beaker followed by ignition from the bottom of the beaker like the eruption of the volcano by forming a dark grey ash type massy product which blow up to the top of the beaker. Thereafter the obtained dark grey ash was ground in an agate mortar for about 2 hours. The resulting powder was calcined for 10 hours at  $950^\circ$  to obtain the pure phase spinel structure of the required nanoferrite powder sample and after calcination the powder sample was then ground for half an hour using an agate mortar to obtain uniform powder. Finally fine brownish dark powder was formed. The synthesis procedures are summarized in Figure 3.1.

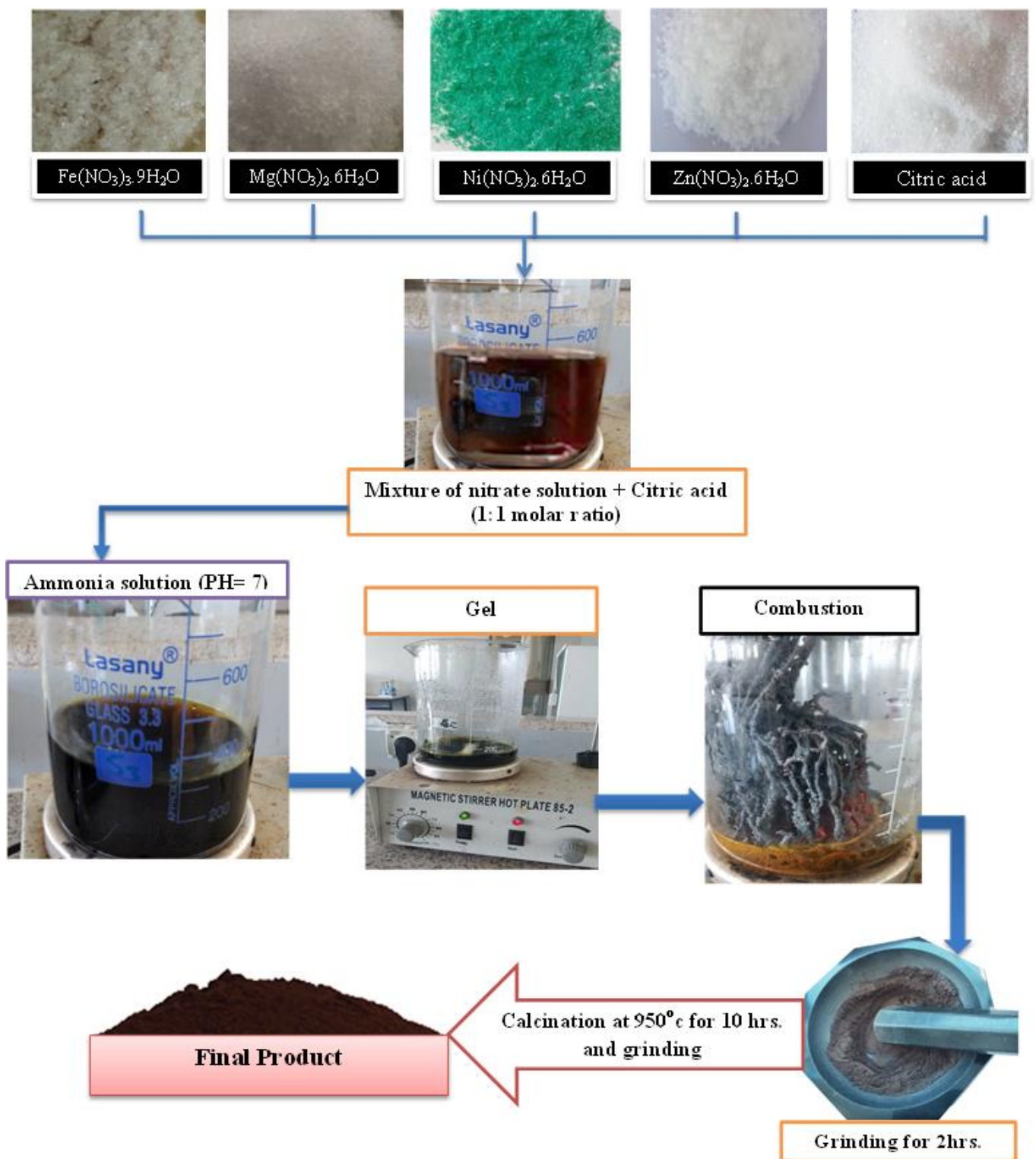


Figure 3.1. Schematic diagram for the preparation of  $\text{Ni}_{0.6}\text{Zn}_{0.4-x}\text{Mg}_x\text{Fe}_2\text{O}_4$  ( $x = 0.0, 0.1, 0.15, 0.2$ ) nanoferrites by sol-gel combustion method.

### 3.3 Material characterization

In this research, the following techniques were utilized to characterize the prepared samples,

- X-Ray Powder Diffraction
- Field Emission Scanning Electron Microscopy
- Fourier Transform Infrared Spectroscopy
- UV-Visible Spectroscopy
- Vibrating Sample Magnetometer

#### 3.3.1 X-Ray power diffraction

X-ray diffraction is a common technique for the study of crystal structures and atomic spacing. X-ray diffraction is based on constructive interference of monochromatic X-rays and a crystalline sample. The position of the peaks will provide the phase formation of the targeted compound. When x-ray strikes a crystal, the electromagnetic wave penetrates the crystal structure. Each plane of atoms in the crystal reflects a portion of the waves. The reflected wave from different planes then interferes with each other and gives rise to a diffraction beam which is at a well-defined angle  $2\theta$  to the incident beam. The incident beam becomes diffracted by the crystal structure. It is observed that some of the incident beam goes through the crystal undiffracted and some of the beam becomes diffracted. Further, it is found that the diffracted rays exist only in certain directions. These diffraction directions correspond to well define diffraction angles  $2\theta$ . The diffraction angle,  $2\theta$ , the wavelength of the x-rays, and the interplanar separation  $d$  of the diffraction planes within the crystal are related through the Bragg diffraction condition, that is,

$$n\lambda = 2d\sin\theta \quad n=1, 2, 3 \dots \quad \text{Bragg's law} \quad \dots\dots\dots (3.1)$$

where  $d$  is the inter-planar distance,  $\theta$  is the Bragg angle,  $n$  is the order of the diffraction and  $\lambda$  is the wavelength of the incident wave [39,40].

In the present work, the structure and face formation of all samples were detected by using characterized using a PANalytic Cu-K $\alpha$  powder diffractometer fitted with Cu-K $\alpha$  radiation ( $\lambda = 1.54060 \text{ \AA}$ ) over a  $2\theta$  range from  $10^\circ$  up to  $80^\circ$ .

The unit cell lattice parameter ( $a$ ,) were calculated by the least square fitting method from the  $d$ -spacing and the Miller indices,  $hkl$  using following relation;

$$a = d \sqrt{h^2 + k^2 + l^2} \dots\dots\dots (3.2)$$

The unit cell volume of the all samples will be calculated by;

$$V = a^3 \dots\dots\dots (3.3)$$

The average crystallite size of the samples will be calculated using Scherrer's formula [41];

$$D = \frac{0.9\lambda}{\beta \cos \theta} \dots\dots\dots (3.4)$$

where  $\lambda$  is the X-ray wavelength,  $\theta$  is the Bragg diffraction angle, and  $\beta$  is the full width half maxima FWHM of the XRD peak appearing at the diffraction angle  $\theta$ .

**3.3.2 Field emission scanning electron microscope**

Field emission electron microscope is a type of material characterization instrument which is just like SEM that images the sample surface by scanning it with higher energy beam of electrons for examination and analysis but with higher resolution and much better energy.

SEM uses a very fine probe of electrons focused at the surface of the specimen and scanned across it in a raster or pattern of parallel lines. It is capable of producing ultrahigh resolution images of a sample surface at low accelerating voltages and small working distance.

Electrons interact with the atoms that make up the sample producing signals which allows an image to be created by analysis of the secondary electrons and back-scattered electrons. Backscattered electrons are rich in surface sensitive information, which is highly important to FE-SEM measurement. The application of FE-SEM can include topography (the surface features of an object and its texture), morphology (the shape and size of the particles making up the object), etc. [42].

In this work, FE-SEM characterization was conducted using JSM-7500F instrument. All samples were coated with platinum before the characterization was conducted.

**3.3.3 Fourier transform infrared spectroscopy**

Fourier transformed infrared (FT-IR) spectroscopy technique is used for investigating the infrared spectra in terms of absorbance or transmittance. In infrared spectroscopy, IR radiation is passed through a sample. Some of the infrared radiation is absorbed by the sample and some of it is passed through (transmitted) [43].



The resulting spectrum represents the molecular absorption and transmission, creating a molecular fingerprint of the sample. Like a fingerprint no two unique molecular structures produce the same infrared spectrum. This makes infrared spectroscopy useful for several types of analysis. So, FTIR can provide some information such as to identify unknown materials, determine the quality or consistency of a sample, and determine the amount of components in a mixture.

In this study, the IR spectra of all the synthesized samples were measured using Shimadzu FT-IR-8900 spectrometer in the wave number region between 1000 cm<sup>-1</sup> and 400 cm<sup>-1</sup>. For this purpose, the prepared four samples were grinded into fine particles in agate mortar and pestle for 5 minutes. These fine particles then were mixed with a IR transparent KBr powder. The resulting powder mixture was transferred into 10mm stainless steel disk for a die set and 5 tons of pressure were applied using a hydraulic press for 4 minute to form a very fine thin pellet [44].

### 3.3.4 Ultraviolet–visible spectroscopy

Ultraviolet–Visible (UV-Vis) spectroscopy is a powerful characterization technique which is used to study the optical properties, such as the optical band gap and refractive index of materials. The term band gap refers to the energy difference between the top of the valence band to the bottom of the conduction band; electrons are able to jump from one band to another. In order for an electron to jump from a valence band to a conduction band, it requires a specific minimum amount of energy for the transition, the band gap energy.

In this study, the optical properties of all synthesized samples will be conducted using UV-Vis spectrophotometer (SPOCORD), analytical Jena, Germany, 190-1110 nm, in the wavelength region of 300 to 800 nm. The optical band gap of these materials was determined using the fundamental absorption, which corresponds to electron excitation from the valence band to the conduction band using Tauc's relation;

$$(\alpha h\nu) = A(h\nu - E_g)^n \dots\dots\dots (3.5)$$

Where  $\alpha$  is the absorption coefficient,  $E_g$ -optical energy gap,  $A$  is a constant which is different for different transitions,  $(h\nu)$  is energy of photon and  $n$  is an index which assumes the values 1/2, 3/2, 2 and 3 depending on the nature of the electronic transition responsible for the reflection [45].

### 3.3.5 Vibrating sample magnetometer

The vibrating sample magnetometer (VSM) has become a widely used characterization technique for investigating the magnetic behavior of magnetic materials. VSM works on Faraday's Law of induction, which informs that a changing magnetic field was produced an electric field and this electric field can be measured and provide us information about the induced magnetic field in the material. The room temperature magnetization of all samples will be measured using vibrating sample magnetometer system (VSM 3900 Princeton) instrument. The external magnetic field was applied in the range of -10,000 to 10,000 Gauss [46].

The magnetic property of the synthesized four samples of  $\text{Ni}_{0.6}\text{Zn}_{0.4-x}\text{Mg}_x\text{Fe}_2\text{O}_4$  ( $x = 0.0, 0.1, 0.15, 0.2$ ) nanoferrites were measured by using a vibrating sample magnetometer system (VSM 3900 Princeton) instrument. The external magnetic field was applied in the range of -10,000 to 10,000 Oe.

## CHAPTER FOUR

### RESULT AND DISSCUTION

In this chapter, the main results and discussion of the synthesized  $\text{Ni}_{0.6}\text{Zn}_{0.4-x}\text{Mg}_x\text{Fe}_2\text{O}_4$  ( $x = 0.0, 0.1, 0.15, \text{ and } 0.2$ ) nanoferrites are discussed. The physical properties including structural, optical, and magnetic properties of the investigated materials are briefly explained.

#### 4.1. X-ray powder diffraction analysis

The phase formation and the crystalline structure of the synthesized  $\text{Ni}_{0.6}\text{Zn}_{0.4-x}\text{Mg}_x\text{Fe}_2\text{O}_4$  ( $x = 0.0, 0.1, 0.15, \text{ and } 0.2$ ) ferrite nanoparticles was identified by using X-ray powder diffraction (XRD) technique in the range of  $2\theta$  between  $10^\circ$  and  $80^\circ$  after the sample is calcined at  $950^\circ\text{C}$  for 10 hours. The room temperature XRD patterns of  $\text{Ni}_{0.6}\text{Zn}_{0.4-x}\text{Mg}_x\text{Fe}_2\text{O}_4$  ( $x = 0.0, 0.1, 0.15, \text{ and } 0.2$ ) nanoferrite in the form of powder are shown in Figure 4.1. All these samples were synthesized by sol-gel combustion method. As shown in the figure, a well-defined XRD patterns and sharp peaks are formed from all the synthesized powder samples, indicating the good degree of the crystallinity nature of all samples. Secondary phase or extra peak (represented by \*) was observed due to the presence of  $\text{Fe}_2\text{O}_3$  in all samples at around  $33.2^\circ$ . Such peaks were also detected in earlier report about  $\text{Ni}_{1-x}\text{Zn}_x\text{Fe}_2\text{O}_4$  samples [47].

Moreover, the diffraction peaks in all samples are indexed as (111), (220), (311), (222), (400), (422), (511), and (440) planes. All these peaks are well matched with the spinel cubic structure of nickel zinc ferrite (JCPDS card no. 08-0234 powder diffraction file) with a  $\text{Fd-}3\text{m}$  space group. This confirms that Mg metal substitution into does not change the cubic structure of  $\text{Ni}_{0.6}\text{Zn}_{0.4}\text{Fe}_2\text{O}_4$ . The broader peaks are also observed in all samples, which confirm the formation of the nanosized particles of the materials under investigation. In comparison to  $\text{Ni}_{0.6}\text{Zn}_{0.4}\text{Fe}_2\text{O}_4$  nanoferrite (Figure 4,2), the XRD diffraction peaks are slightly shifted towards the higher diffraction angles with an increase in Mg content up to  $x = 0.15$ , after which it is shifted to the lower angles with a further addition of Mg content. This is associated with the change in lattice parameters as well as unit cell volumes of  $\text{Ni}_{0.6}\text{Zn}_{0.4}\text{Fe}_2\text{O}_4$  nanoferrites, indicating the incorporation of Mg into  $\text{Ni}_{0.6}\text{Zn}_{0.4}\text{Fe}_2\text{O}_4$  lattice.

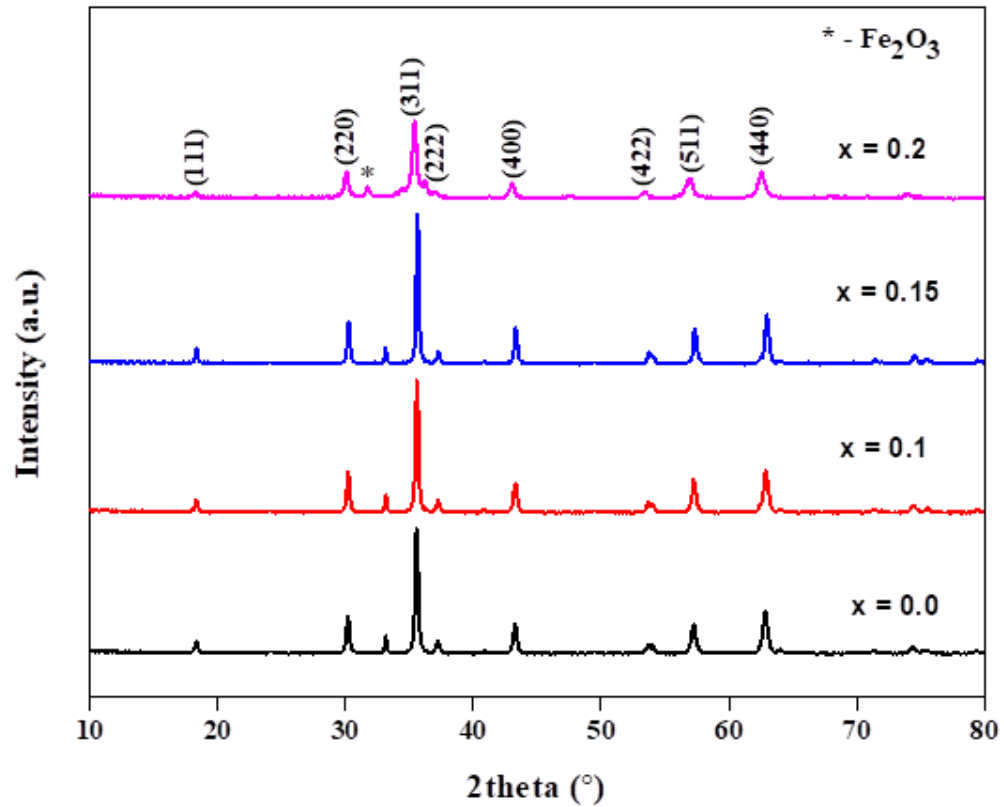


Figure 4.1. XRD patterns for  $\text{Ni}_{0.6}\text{Zn}_{0.4-x}\text{Mg}_x\text{Fe}_2\text{O}_4$  nanoferrites.

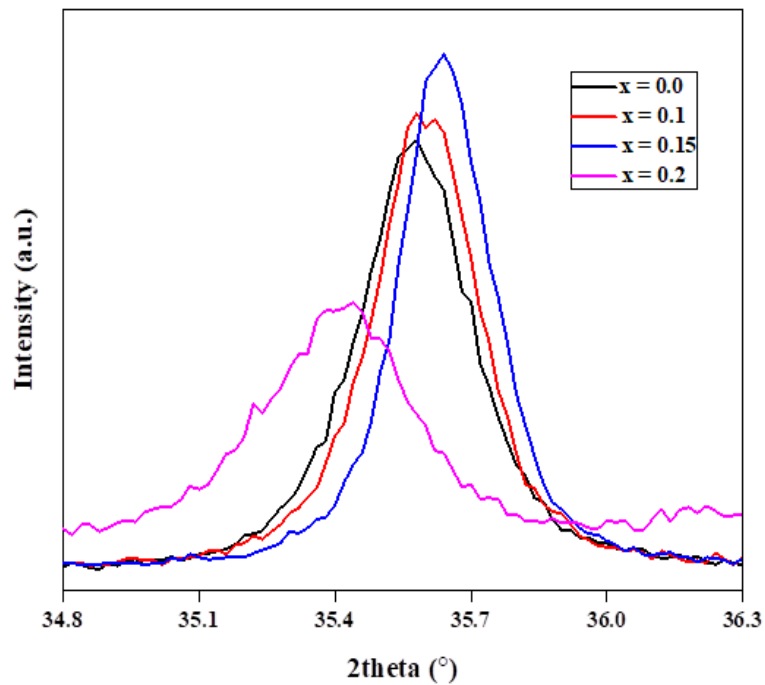


Figure 4.2. Shifting of the (311) XRD peaks for  $\text{Ni}_{0.6}\text{Zn}_{0.4-x}\text{Mg}_x\text{Fe}_2\text{O}_4$  nanoferrites.

In order to investigate the effect of Mg cation substitution for Zn cation on the structural parameters of  $\text{Ni}_{0.6}\text{Zn}_{0.4-x}\text{Mg}_x\text{Fe}_2\text{O}_4$  ferrite nanoparticles, the lattice parameters as well as the corresponding unit cell volumes were calculated by using Equations 3.2 and 3.3, respectively. The crystal sizes of all samples were also calculated using Debye-Scherer's method from (*hkl*) value of (311) using Equation 3.4. The obtained results are summarized in Table 4.1. It is observed that the lattice parameters and the unit cell volumes of  $\text{Ni}_{0.6}\text{Zn}_{0.4-x}\text{Mg}_x\text{Fe}_2\text{O}_4$  decreased with an increase in Mg content up to  $x = 0.15$ , after which it is increased with a further addition of Mg content ( $x = 0.2$ ). The decreased in the lattice constants and unit cell volume is related to the size of the lower ionic radius of  $\text{Mg}^{2+}$  (0.72 Å) [48] than  $\text{Zn}^{2+}$  (0.84 Å) [49]. However, for spinel  $\text{Ni}_{0.6}\text{Zn}_{0.4-x}\text{Mg}_x\text{Fe}_2\text{O}_4$  with  $x = 0.15$  shows an inverse trend in comparison with the  $\text{LiNi}_{0.5}\text{Co}_{0.5}\text{PO}_4$  sample. This may be related to the structural fluctuation. As shown in Table 4.1. The crystallite sizes vary non-monotonically with an increase in the content of Mg into  $\text{Ni}_{0.6}\text{Zn}_{0.4-x}\text{Mg}_x\text{Fe}_2\text{O}_4$  ferrite nanoparticles. However, a significant increment of crystallite size is obtained for  $\text{Ni}_{0.6}\text{Zn}_{0.25}\text{Mg}_{0.15}\text{Fe}_2\text{O}_4$  sample.

Table 4.1. Structural parameters for  $\text{Ni}_{0.6}\text{Zn}_{0.4-x}\text{Mg}_x\text{Fe}_2\text{O}_4$  nanoferrites.

<b>Mg content (x)</b>	<b>d-spacing for (400) (Å)</b>	<b>2θ value for (311) (degree)</b>	<b>FWHM for (311) (degree)</b>	<b>Lattice Constant from (311) (Å)</b>	<b>Unite Cell Volume V (Å)<sup>3</sup></b>	<b>Crystal Size from (311) D(nm)</b>
0.0	2.08964	35.5849	0.20690	8.3586	583.98	59.4
0.1	2.08871	35.6102	0.25450	8.3548	582.56	58.0
0.15	2.08692	35.6513	0.21350	8.3477	581.70	71.5
0.2	2.10006	35.4135	0.40250	8.4002	592.75	47.5

## 4.2. FE-SEM study

The morphology and particle size distribution are the most important parameters that have a marked influence on the physical properties of ferrite materials. Figure 4.2 shows the FE-SEM micrographs of the synthesized  $\text{Ni}_{0.6}\text{Zn}_{0.4-x}\text{Mg}_x\text{Fe}_2\text{O}_4$  ( $x = 0.0, 0.1, 0.15, \text{ and } 0.2$ ) nanoferrite samples. All samples have nearly spherical shaped grains with some agglomeration. However, significant particle agglomeration is observed in  $\text{Ni}_{0.6}\text{Zn}_{0.2}\text{Mg}_{0.2}\text{Fe}_2\text{O}_4$  nanoferrite. Large sized grains ( $0.53\mu\text{m}$ ) are also observed in  $\text{Ni}_{0.6}\text{Zn}_{0.25}\text{Mg}_{0.15}\text{Fe}_2\text{O}_4$  nanoferrite, which is in good agreement with the sizes we obtained from XRD study. The average grain sizes for all samples were calculated by using imageJ software, and they are found to be in the range between  $0.27$  to  $0.53\mu\text{m}$ , indicating that the obtained grain sizes are found to be larger than the crystallite sizes calculated from XRD analysis. This confirms that grain sizes are larger than crystallite size as it contains a number of crystallites.

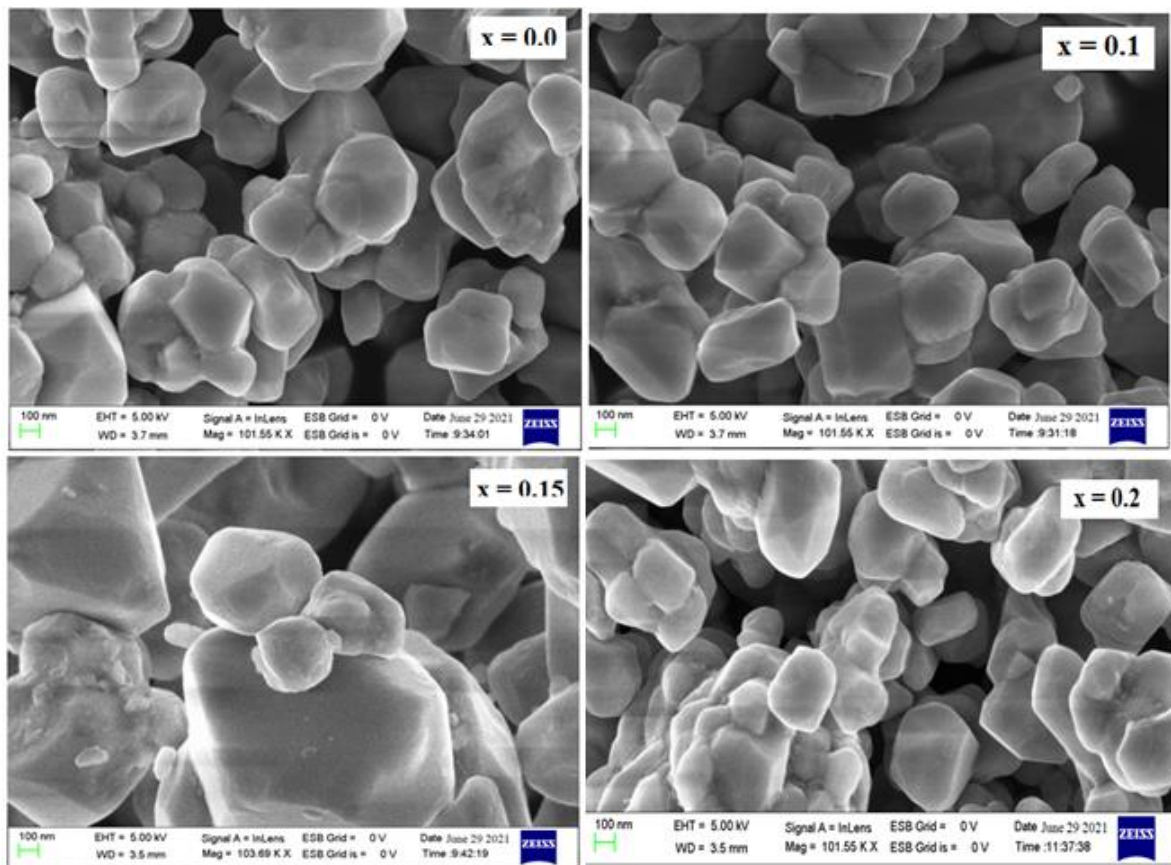


Figure 4.3. FE-SEM images for  $\text{Ni}_{0.6}\text{Zn}_{0.4-x}\text{Mg}_x\text{Fe}_2\text{O}_4$  nanoferrites.

### 4.3. FT-IR spectroscopy study

Figure 4.4 shows the room temperature FT-IR spectroscopy analysis of  $\text{Ni}_{0.6}\text{Zn}_{0.4-x}\text{Mg}_x\text{Fe}_2\text{O}_4$  ( $x = 0.0, 0.1, 0.15, \text{ and } 0.2$ ) ferrite nanoparticles in the form of powder synthesized by sol-gel combustion method. The obtained vibrational band values are summarized in Table 4.2. It is known that in spinel cubic based ferrite materials, two distinct absorption metal-oxygen bands are formed in the FT-IR spectra. One is at around a wavelength of  $600\text{ cm}^{-1}$  and the other is at around  $400\text{ cm}^{-1}$ . The frequency band at  $600\text{ cm}^{-1}$  is caused by the stretching vibration of the metal-oxygen bands in the tetrahedral sites, while the one at around  $400\text{ cm}^{-1}$  is caused by the stretching vibration of oxygen-metal ions in the octahedral sites [50, 51]. In this study, all samples exhibit different absorption spectral in between  $596.2\text{ cm}^{-1}$  and  $429.7\text{ cm}^{-1}$ . The bands observed at around  $600\text{ cm}^{-1}$  are attributed to metal-oxygen the intermolecular vibrations of the  $\text{MO}_4$  ( $M = \text{metal}$ ) molecules in the tetrahedral sites [52]. While, the bands observed at around  $400\text{ cm}^{-1}$  are attributed to the asymmetric stretching modes of  $\text{MO}_6$  ( $M = \text{metal}$ ) in the octahedral sites [53]. The formations of bands also verify the formation of spinel phase ferrites.

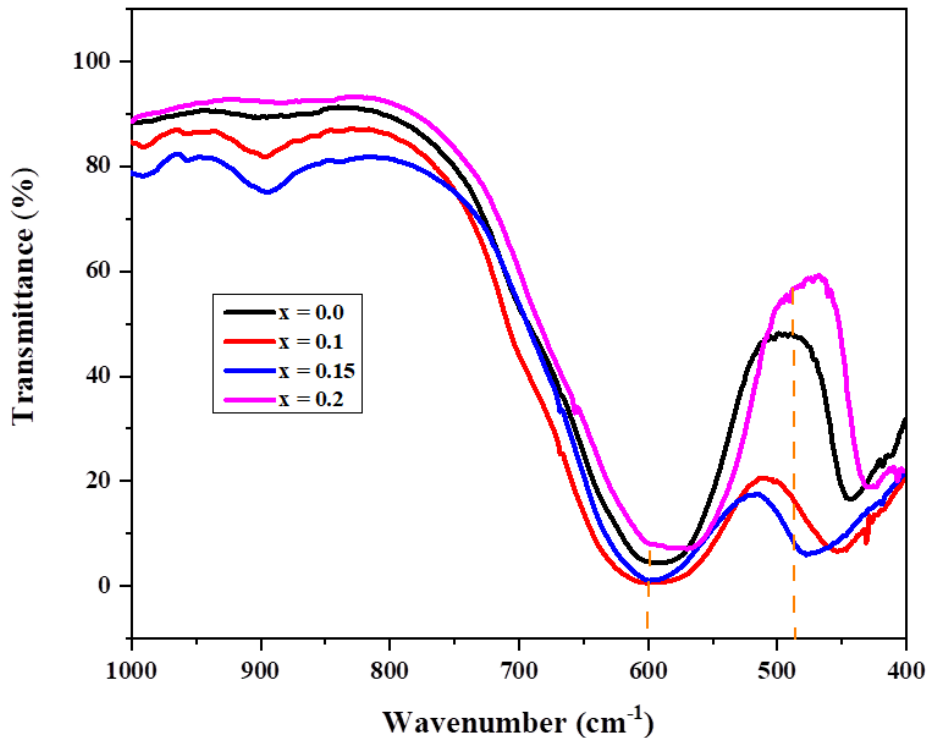


Figure 4.4. FT-IR spectra for  $\text{Ni}_{0.6}\text{Zn}_{0.4-x}\text{Mg}_x\text{Fe}_2\text{O}_4$  nanoferrites.

In comparison with the  $\text{Ni}_{0.6}\text{Zn}_{0.4}\text{Fe}_2\text{O}_4$  sample, the peaks of Mg substituted samples with a concentration of  $x = 0.1$  and  $x = 0.15$  are shifted slightly towards a higher wavenumber regions. The shifting of the bands towards higher wavenumber with an increase in the concentration of  $\text{Mg}^{2+}$  ions is attributed to the increase in the unit cell dimensions as evidenced by the variation in the lattice constant. The increase in the unit cell dimensions affects the metal-oxygen ions, which is in agreement with the shift we observed from XRD results. Thus, the shift in the peak position to the higher wavenumber indicate that the substitution of Mg for Zn ions increase the bond strength of the metal-oxygen ions in the  $\text{Ni}_{0.6}\text{Zn}_{0.3}\text{Mg}_{0.1}\text{Fe}_2\text{O}_4$  and  $\text{Ni}_{0.6}\text{Zn}_{0.25}\text{Mg}_{0.15}\text{Fe}_2\text{O}_4$  lattices. It is also in good agreement with their lower lattice parameter and unit cell volume of calculated from the obtained XRD pattern. For  $\text{Ni}_{0.6}\text{Zn}_{0.2}\text{Mg}_{0.2}\text{Fe}_2\text{O}_4$  sample, the two bands are shifted to the lower wavelength to that of  $\text{Ni}_{0.6}\text{Zn}_{0.4}\text{Fe}_2\text{O}_4$  sample. This is also related to the size of its unit cell volume. As shown in the Table 4.2 and Figure 4.4, significant change in the positions of bands is observed in the tetrahedral sites, suggesting that the substituted Mg cations are largely incorporated to these sites in the  $\text{Ni}_{0.6}\text{Zn}_{0.25}\text{Mg}_{0.15}\text{Fe}_2\text{O}_4$  lattices.

Table 4.2. Tetrahedral ( $\nu_1$ ) and Octahedral ( $\nu_2$ ) absorption bands of  $\text{Ni}_{0.6}\text{Zn}_{0.4-x}\text{Mg}_x\text{Fe}_2\text{O}_4$  nanoferrites.

<b>Mg content (x)</b>	<b><math>\nu_1</math> (<math>\text{cm}^{-1}</math>)</b>	<b><math>\nu_2</math> (<math>\text{cm}^{-1}</math>)</b>
<b>0.0</b>	591.3	441.8
<b>0.1</b>	593.5	453.2
<b>0.15</b>	596.2	476.7
<b>0.2</b>	578.6	427.2

#### 4.4. Optical property study

UV-Vis spectra analysis has been widely used to investigate the optical properties of spinel ferrite nanoparticles. Different studies reported that as the particle size of crystals decreases, the absorption edge shifts to shorter wavelength, due to the band gap increase of the smaller particles [49]. In this study, the optical properties of the  $\text{Ni}_{0.6}\text{Zn}_{0.4-x}\text{Mg}_x\text{Fe}_2\text{O}_4$  ( $x = 0.0, 0.1, 0.15,$  and  $0.2$ ) nanoferrite was investigated by UV-Vis absorption spectrum recorded in the range of 300-800 nm.



Figure 4.5 shows the UV-Vis absorption spectra of the synthesized ferrite nanoparticles. As shown in the figure, all the synthesized samples have low absorbance in visible region and high absorbance in ultraviolet region. This indicates that  $\text{Ni}_{0.6}\text{Zn}_{0.4-x}\text{Mg}_x\text{Fe}_2\text{O}_4$  ( $x = 0.0, 0.1, 0.15,$  and  $0.2$ ) ferrite nanoparticles are optically activated under ultraviolet light region. The strong absorption peaks in the ultraviolet regions of wavelength implies that there exists a strong electronic excitation from the valance band to conduction band in all samples mainly due to ultraviolet light radiation. Different slopes are also seen at a different wavelength, which may be related to different electron transitions between cations and oxygen ions in the  $\text{Ni}_{0.6}\text{Zn}_{0.4-x}\text{Mg}_x\text{Fe}_2\text{O}_4$  lattice. The absorption band further decrease gradually as the wavelength increases. Moreover, the position of the absorption bands are related to the crystallite sizes of the  $\text{Ni}_{0.6}\text{Zn}_{0.4-x}\text{Mg}_x\text{Fe}_2\text{O}_4$  ( $x = 0.0, 0.1, 0.15,$  and  $0.2$ ) ferrite nanoparticles.

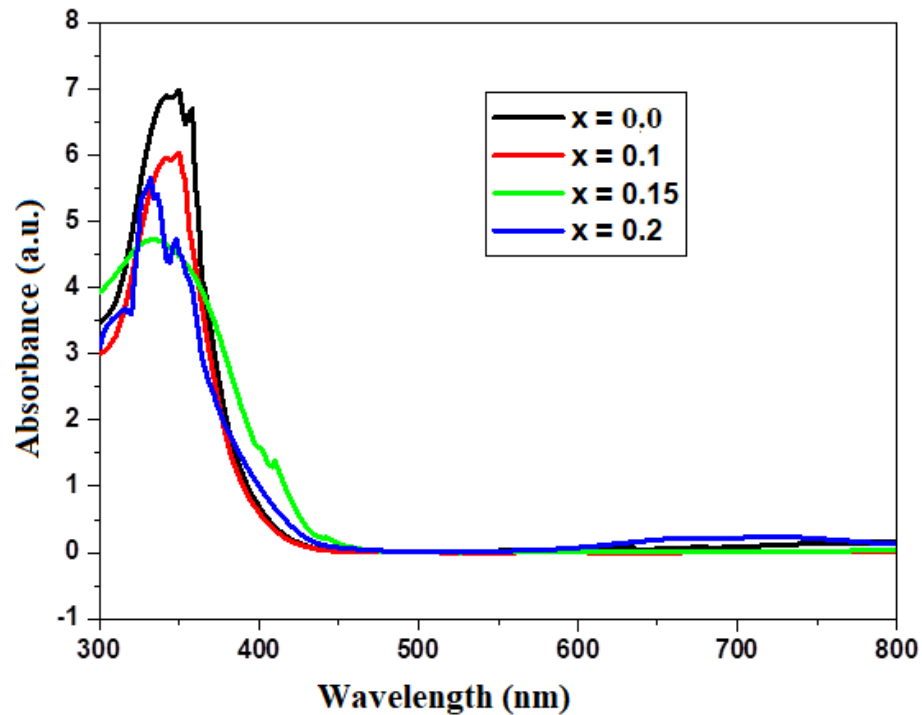


Figure 4.5. UV-Vis absorbance spectra for  $\text{Ni}_{0.6}\text{Zn}_{0.4-x}\text{Mg}_x\text{Fe}_2\text{O}_4$  nanoferrites.

The optical energy band gap for  $\text{Ni}_{0.6}\text{Zn}_{0.4-x}\text{Mg}_x\text{Fe}_2\text{O}_4$  ( $x = 0.0, 0.1, 0.15,$  and  $0.2$ ) nanoferrites were estimated by using Tauc's relation (Equation 4.5). To obtain the optical band gap of all samples, the graph of  $(\alpha h\nu)^{1/2}$  versus  $h\nu$  was plotted, and the plot is shown in Figure 4.5. The intercept of the line at  $\alpha = 0$  gives the value of optical band gap energy of all samples.

The optical band gap energies of  $\text{Ni}_{0.6}\text{Zn}_{0.4-x}\text{Mg}_x\text{Fe}_2\text{O}_4$  ferrite nanoparticles with  $x = 0.0, 0.1, 0.15,$  and  $0.2$  are found to be  $1.77, 1.79, 1.7,$  and  $1.83$  eV, respectively, which are in a good agreement with the reported values [54]. It has been reported that the optical band gap of materials is affected by different factors, such as crystallite size, lattice parameter, and presence of impurities [54]. In this study, the variation in the optical band gap observed in all samples is related with the crystallite sizes of samples. A sample which has the largest crystallite size ( $\text{Ni}_{0.6}\text{Zn}_{0.4-x}\text{Mg}_x\text{Fe}_2\text{O}_4 = 71.5$  nm) possessed the lowest band gap energy ( $1.7$  eV), while a sample which has the lowest crystallite size ( $\text{Ni}_{0.6}\text{Zn}_{0.4-x}\text{Mg}_x\text{Fe}_2\text{O}_4 = 47.5$  nm) delivered the largest band gap energy ( $1.83$  eV) [49]. Moreover, the obtained values of the band gaps energy indicate all the synthesized samples have a semiconductor behavior due to the obtained band gaps are found to be in the range of the band gap of semiconductor materials ( $1$  to  $4$  eV).

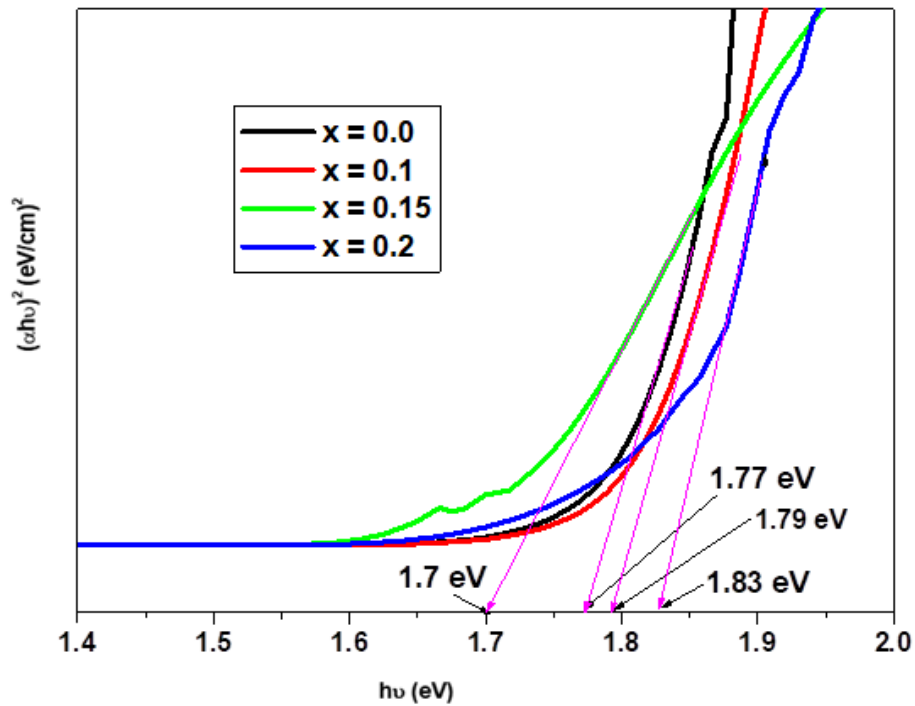


Figure 4.6. Tauc plot for  $\text{Ni}_{0.6}\text{Zn}_{0.4-x}\text{Mg}_x\text{Fe}_2\text{O}_4$  nanoferrites.

#### 4.5. Magnetic properties study

The room temperature magnetic properties of  $\text{Ni}_{0.6}\text{Zn}_{0.4-x}\text{Mg}_x\text{Fe}_2\text{O}_4$  ( $x = 0.0, 0.1, 0.15,$  and  $0.2$ ) nanoferrites were characterized by using vibrating sample magnetometer with an applied magnetic field between  $-10,000$  and  $10,000 \text{ O}_e$ .

The obtained magnetic hysteresis curves of all samples are shown in Figure 4.6. From the magnetic hysteresis loops, different magnetic parameters, like saturation magnetization ( $M_s$ ), remnant magnetization ( $M_r$ ) and coercivity ( $H_c$ ), and squareness ratio ( $M_r/M_s$ ) of the samples can be determined. The evaluated magnetic parameters are recorded in Table 4.3.

As it is observed from the figure, all the synthesized ferrite materials display soft magnetization behavior and normal s-shaped narrow hysteresis loops which confirmed the formation of spinel ferrites. The magnetic behavior of all samples is originated from the magnetic moment of anti-parallel spins between  $\text{Fe}^{3+}$  and  $\text{Ni}^{2+}$  at the tetrahedral and octahedral sites. Because, Mg and Zn ions are nonmagnetic in nature. Among all samples,  $\text{Ni}_{0.6}\text{Zn}_{0.4}\text{Fe}_2\text{O}_4$  delivers a narrower hysteresis loop, indicating that the material can be easily demagnetized. This is associated to  $\text{Zn}^{2+}$  has no unpaired electrons and behaves as paramagnetic as a result the super exchange interaction is low. However, the magnetization curve of the Mg cations substituted samples show a strong ferromagnetic behavior.

It is clear that the magnetic behaviors in spinel ferrites are significantly influenced by numerous factors such as the variations in the magnetic moments, variation in the crystallites size, variations in the concentration and nature of ions in tetrahedral (A) and octahedral (B) sites and synthesis method [55]. The magnetization of the ferrites is derived from the  $\text{Fe}^{3+}$  ions and is principally governed by their distributions in the crystal lattice sites. Besides, it is well known that the A–A and B–B interactions are very weak however the A–B exchange interaction is predominant over them [55].

It is observed that, the saturation magnetization found to decrease with Mg concentration into  $\text{Ni}_{0.6}\text{Zn}_{0.4-x}\text{Mg}_x\text{Fe}_2\text{O}_4$  ( $x = 0.0, 0.1, 0.15,$  and  $0.2$ ) ferrite nanoparticles. The decrease of the saturation magnetization with an increase in Mg concentration may be due to the misbalance of  $\text{Fe}^{3+}$  ions in octahedral and tetrahedral sites, and super exchange interactions conducted in the  $\text{Ni}_{0.6}\text{Zn}_{0.4-x}\text{Mg}_x\text{Fe}_2\text{O}_4$  ( $x = 0.0, 0.1, 0.15,$  and  $0.2$ ) ferrite nanoparticles. It is also observed that the magnetic properties such as remnant magnetization and squareness ratio of Mg substituted samples is greater than to that of  $\text{Ni}_{0.6}\text{Zn}_{0.4}\text{Fe}_2\text{O}_4$ , sample.

This indicates that there is an increase in the ferromagnetic behavior for  $\text{Ni}_{0.6}\text{Zn}_{0.4-x}\text{Mg}_x\text{Fe}_2\text{O}_4$  samples due to the substitution of Mg cations.

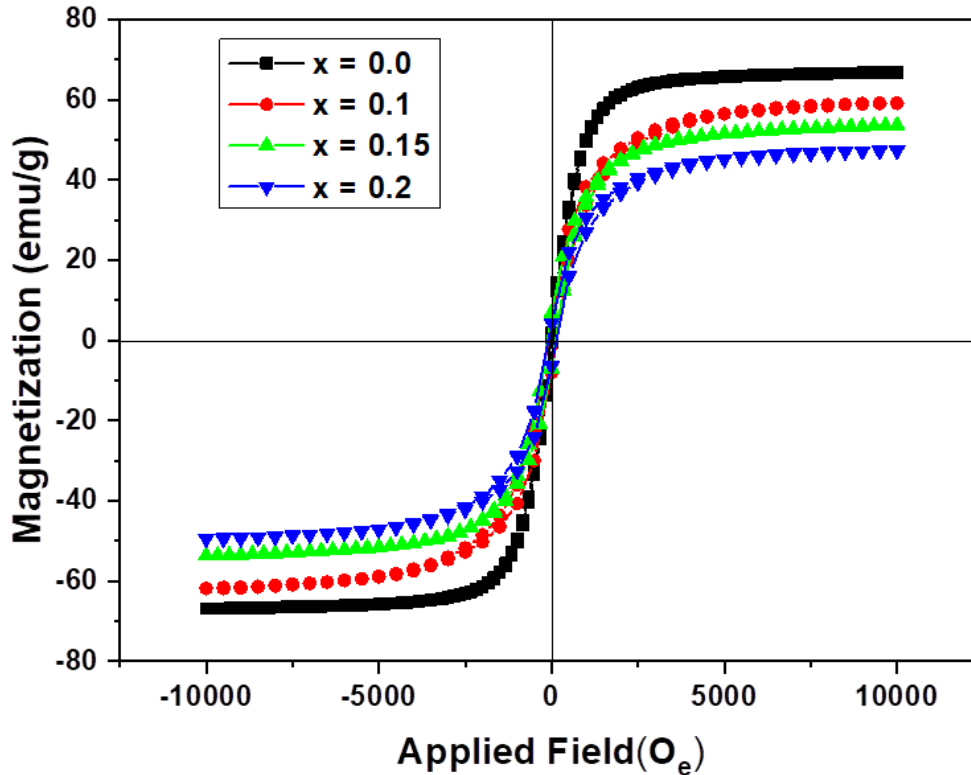


Figure 4.7. Hysteresis curves for  $\text{Ni}_{0.6}\text{Zn}_{0.4-x}\text{Mg}_x\text{Fe}_2\text{O}_4$  nanoferrites.

The variation in coercivity with Mg content is clearly observed in the magnified view of the hysteresis curves in Figure 4.7. It is found that the coercivity of Mg substituted samples is greater than to that of  $\text{Ni}_{0.6}\text{Zn}_{0.4}\text{Fe}_2\text{O}_4$ , sample. This also indicates that there is an increase in the ferromagnetic behavior for  $\text{Ni}_{0.6}\text{Zn}_{0.4-x}\text{Mg}_x\text{Fe}_2\text{O}_4$  samples due to the substitution of Mg cations. In general, the observed ferromagnetism in Mg substituted samples could be due to super exchange interaction between cations at tetrahedral and octahedral sites. This means that substitution of magnetic ion such as Mg results in the improvement in the exchange interaction between tetrahedral and octahedral sites, which results in the strengthening of A-B interaction in ferrites samples.

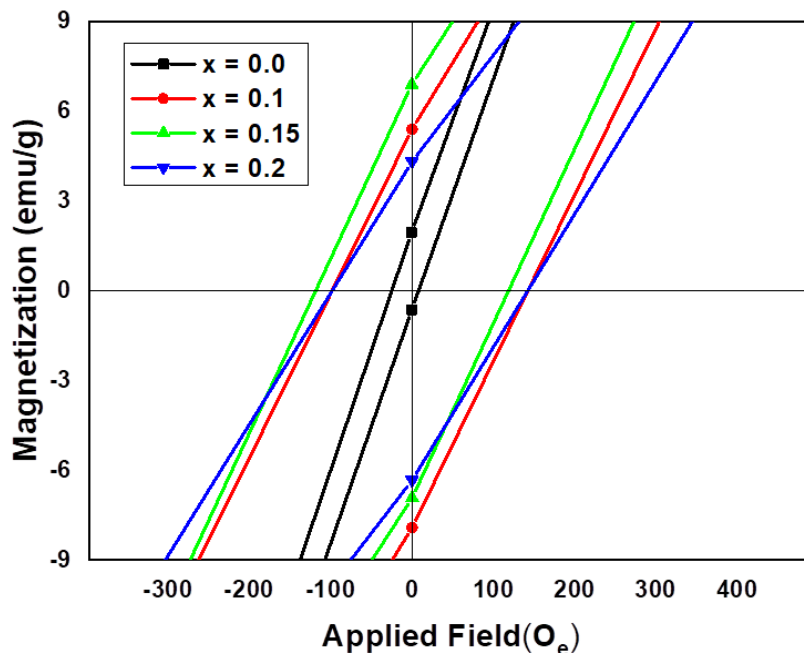


Figure 4.8: The magnified view of hysteresis loops of  $\text{Ni}_{0.6}\text{Zn}_{0.4-x}\text{Mg}_x\text{Fe}_2\text{O}_4$  nanoferrites.

As shown in Table 4.4, The squareness ratio ( $M_r/M_s$ ) values of all samples were found to be less than 0.5, indicating the formation of multi-domain grains. This means that all samples contain a multi-domain structure constituted by regions of uniform magnetization separated by domain walls [56].

Table 4.3: Saturation magnetization ( $M_s$ ), remanent magnetization ( $M_r$ ), coercivity ( $H_c$ ), and squareness ratio ( $M_r/M_s$ ) of all samples.

Mg content (x)	$M_s$ (amu/g)	$M_r$ (amu/g)	$H_c$ (Oe)	$M_r/M_s$
0.0	66.5	1.8	25.6	0.03
0.1	58.7	5.0	141.8	0.09
0.15	53.4	6.4	140.6	0.12
0.2	46.8	4.0	116.3	0.09

## CHAPTER FIVE

### CONCLUSION AND RECOMMENDATION

#### 5.1. Conclusion

In this research,  $\text{Ni}_{0.6}\text{Zn}_{0.4-x}\text{Mg}_x\text{Fe}_2\text{O}_4$  nanoferrites were synthesized by using sol-gel combustion method using Nickel nitrate, Zinc nitrate, Magnesium nitrate and ferric nitrate precursors. Citric acid was also used as a fuel and chelating agent during the synthesis process. The structural, optical and magnetic properties of these materials were conducted using XRD, FE-SEM, FT-IR spectroscopy, UV-Vis spectroscopy and Vibrating sample magnetometer.

The XRD and FT-IR analysis study confirmed the formation of single-phase cubic spinel structured materials. From the XRD analysis, it was identified that slight changes in the lattice constant, unit cell volume, and crystallite size were observed due to the substitution of Mg into  $\text{Ni}_{0.6}\text{Zn}_{0.4-x}\text{Mg}_x\text{Fe}_2\text{O}_4$  ferrite nanoparticles. It was identified that the lattice parameters and the unit cell volumes of the synthesized samples decreased with an increase in Mg content up to  $x = 0.15$ , after which it was increased with a further addition of Mg content ( $x = 0.2$ ). The crystallite sizes varied non-monotonically with an increase in the content of Mg into  $\text{Ni}_{0.6}\text{Zn}_{0.4-x}\text{Mg}_x\text{Fe}_2\text{O}_4$  ferrite nanoparticles, and they were found between 47.5 and 71.5 nm, indicating that all the synthesized materials possessed a nanocrystalline structure. The FE-SEM micrographs confirmed that all samples have porous structure and nearly spherical shaped grains with some agglomeration. From FT-IR measurements, two strong absorption bands were identified in the IR spectra of all samples. The higher frequency bands  $\nu_1$  which appeared between 583.0 and 596.2  $\text{cm}^{-1}$  are assigned to the stretching vibration of the metal-oxygen ions in the tetrahedral sites. While the lower frequency bands  $\nu_2$  which appeared between 429.7 and 476.7  $\text{cm}^{-1}$  are assigned to the stretching vibration of the metal-oxygen ions in the octahedral sites.

From the optical property study, it was identified that all the synthesized samples are optically activated under ultraviolet light. The optical band gap energies were found between 1.7 and 1.83 eV,  $\text{Ni}_{0.6}\text{Zn}_{0.2}\text{Mg}_2\text{Fe}_2\text{O}_4$  sample possessed the highest band gap energy (1.83 eV) associated with its lowest crystallite size (47.5 nm). The magnetic property study confirmed the soft magnetization behavior of the synthesized samples at room temperature.

The saturation magnetization was reduced from 66.5 to 46.8 emu/g when the content of Mg ions increased from  $x = 0.15$  to  $x = 0.2$  in  $\text{Ni}_{0.6}\text{Zn}_{0.4-x}\text{Mg}_x\text{Fe}_2\text{O}_4$  compound.

The loop squareness ratio ( $M_r/M_s$ ) of all samples were found to be less than 0.5, indicating that  $\text{Ni}_{0.6}\text{Zn}_{0.4-x}\text{Mg}_x\text{Fe}_2\text{O}_4$  ( $x = 0.0, 0.1, 0.15, \text{ and } 0.2$ ) nanoferrites may be used for cores and coils with low inductance applications.

## 5.2. Recommendation

In this study, attempts were made to investigate the structure, optical, and magnetic properties of  $\text{Ni}_{0.6}\text{Zn}_{0.4-x}\text{Mg}_x\text{Fe}_2\text{O}_4$  ( $x = 0.0, 0.1, 0.15, \text{ and } 0.2$ ) nanoferrites prepared by the sol-gel combustion method. Based on the findings of this work, the following issues are forwarded as recommendation:

1. Sol-gel combustion synthesis is an effective method to produce  $\text{Ni}_{0.6}\text{Zn}_{0.4-x}\text{Mg}_x\text{Fe}_2\text{O}_4$  ( $x = 0.0, 0.1, 0.15, \text{ and } 0.2$ ) nanoferrites using  $\text{Ni}(\text{NO}_3)_2 \cdot 6\text{H}_2\text{O}$ ,  $\text{Zn}(\text{NO}_3)_2 \cdot 6\text{H}_2\text{O}$ ,  $\text{Mg}(\text{NO}_3)_2 \cdot 6\text{H}_2\text{O}$ ,  $\text{Fe}(\text{NO}_3)_3 \cdot 9\text{H}_2\text{O}$  and  $\text{C}_6\text{H}_8\text{O}_7 \cdot \text{H}_2\text{O}$  precursors. The amount of calcination temperature ( $950^\circ\text{C}$ ) and calcination time (10 hours) are compatible for producing  $\text{Ni}_{0.6}\text{Zn}_{0.4-x}\text{Mg}_x\text{Fe}_2\text{O}_4$  ( $x = 0.0, 0.1, 0.15, \text{ and } 0.2$ ) nanoferrites.
2.  $\text{Ni}_{0.6}\text{Zn}_{0.4-x}\text{Mg}_x\text{Fe}_2\text{O}_4$  ( $x = 0.0, 0.1, 0.15, \text{ and } 0.2$ ) nanoferrites were optically activated under ultraviolet light. Thus, the synthesized samples may be used as ultraviolet radiation sensor.
3. The loop squareness ratio ( $M_r/M_s$ ) of all samples were found in the range between 0.03 and 0.12, indicating that  $\text{Ni}_{0.6}\text{Zn}_{0.4-x}\text{Mg}_x\text{Fe}_2\text{O}_4$  ( $x = 0.0, 0.1, 0.15, \text{ and } 0.2$ ) ferrite nanoparticles may be used for cores and coils with low inductance applications.
4. In this study, the electrical and dielectric properties of the synthesized samples were not investigated. Therefore, this has to be considered in future study for additional understanding and giving tangible conclusion on the investigated samples.

## REFERENCES

- [1] S. J. Kumar and P. Prameela, “Structural and Magnetic Properties of Copper-Substituted Nickel – Zinc Nanoparticles Prepared by Sol-Gel Method,” 2020.
- [2] A.E. Virden and K. O’Grady, “Structure and magnetic properties of NiZn ferrite nanoparticles,” *Journal of Magnetism and Magnetic Material.*, vol. 290-291 PA, pp. 868–870, 2005.
- [3] K. Velmurugan, V. Sangli, and K. Venkatachalapathy, “Synthesis of Nickel Zinc Iron Nanoparticles by Coprecipitation Technique 2 . Experimental Procedure,” vol. 13, no. 3, pp. 299–303, 2010.
- [4] G. S. Shahane, A. Kumar, M. Arora, R. P. Pant, and K. Lal, “Synthesis and characterization of Ni – Zn ferrite nanoparticles,” *Journal of Magnetism and Magnetic Materials.*, vol. 322, no. 8, pp. 1015–1019, 2010.
- [5] J. H. LIU, L. WANG, F. S. LI, “Magnetic properties and Mossbauer studies of nanosized NiFe<sub>2</sub>O<sub>4</sub> particles,” *Journal of Material Science.*, vol 40, pp. 2573 – 2575, 2005.
- [6] NadeemBaig, Irshad Kammakam and Wail Falath, “Nanomaterials: a review of synthesis methods,properties, recent progress, and challenges” vol.2, no.1821, 2021.
- [7] D. R. S. Gangaswamy<sup>1,3</sup> · M. ChaitanyaVarma , S. Bharadwaj ,K. SambasivaRao, K. H. Rao, “Comparison Study of Structural and Magnetic Propertiesof Magnesium-Substituted Nickel–Zinc Ferrites Synthesized by Solid-State and Sol–Gel Routes”. *Journal of Superconductivity and Novel Magnetism.*,vol. 28, pp.3599–3606, 2015.
- [8] “Chapter one introduction 1. Introduction 1.1 Ferrites,” pp. 1–49, 2014.
- [9] M. F. Huq, D. K. Saha, R. Ahmed, and Z. H. Mahmood, “Ni-Cu-Zn Ferrite Research : A Brief Review,” vol. 5, no. 2, pp. 215–233, 2013.
- [10] Arvinad Kumar, “*Synthesis and characterization of manganese zinc ferrite*”, 2010.
- [11] RichaSrivastava& B. C. Yadav, “Ferrite Materials: Introduction, Synthesis Techniques,and Applications as Sensors” *International Journal of Green Nanotechnology.*, pp. 141-154, 2012.
- [12] Robert C. Pullar, “Synthesis, Properties and Applications of Hexaferrite ceramics: A brief Review,” *Progress in Materials Science.*,” vol. 57, pp. 1191–1334, 2012.
- [13] MubsherHussain, “Fabrication and characterization of cobalt and chromium doped



- strontium based X-type hexagonal ferrites synthesized via micro-emulsion route”
- [14] R.C. Pullar, Prog. “A review of the synthesis, properties and applications of hexaferrite ceramics” *Journal of Progress in Material Science*. 57 (2012) 1191-1334.
- [15] Roberto Nistico, “Magnetic materials and water treatments for a sustainable future” vol. 24, pp.10129, 2017.
- [16] A.P.G. Rodrigues, D.K.S. Gomes, J.H. Araújo, D.M.A. Mela, N.A.S. Oliveira, R.M. Braga, “ Nanoferrites of nickel doped with cobalt: Influence of  $\text{Co}^{2+}$  on the structural and magnetic properties,” *Journal of Magnetism and Magnetic Material*. Vol.374, pp748-754, 2015.
- [17] Z. Yan, J. Luo, “Effect of Ce-Zn Co substitution on the structure, magnetic and microwave absorption properties of nickel ferrite,” *Journal of Alloys and Compound*. Vol.695, pp.1185-1195, 2017.
- [18] R. Aakash, D. Choubey, S. Das, J. Mukerjee, “Effect of doping of manganese ions on the structural and magnetic properties of nickel ferrite, ” *Journal of Alloys and Compound*., vol. 668, pp.33-39, 2016.
- [19] T. Marinca, “Structural and magnetic properties of nanocrystalline  $\text{ZnFe}_2\text{O}_4$  powder synthesized by reactive ball milling Structural and magnetic properties of nanocrystalline  $\text{ZnFe}_2\text{O}_4$  powder synthesized by reactive ball milling,” vol. 5, no.1, pp. 39–43, 2014.
- [20] V. Jeseentharani, M. George, B. Jeyaraj, A. Dayalan, and K. S. Nagaraja, “Synthesis of metal ferrite ( $\text{MFe}_2\text{O}_4$ , M = Co, Cu, Mg, Ni, Zn) nanoparticles as humidity sensor materials,” *Journal of Experimental Nanoscience*., vol. 8, no. 3, pp. 358–370, 2013.
- [21] D.H. Taffa, R. Dillert, AC Ulpe, K.C.L. Bauerfeind, T. Bredow, D.W. Bahnemann, M. Wark, “ Photoelectrochemical and theoretical investigations of spinel type ferrites,” *Journal of Photonics for Energy*., vol. 7(1). pp.01, 2016.
- [22] D. B. Fahad, “Structural , Electrical and Optical Properties of  $\text{Cu}_{1-y}\text{Fe}_y\text{Fe}_2\text{O}_4$  Ferrite System,” *Journal of Physics*. vol. 11, no. 21, pp. 102–109, 2014.
- [23] H. S. Singh and N. Sangwa, “Structural and Magnetic Properties of Nickel Ferrite Nanoparticles Synthesized by Ball Milling,” vol. 6, no. 10, pp. 36–39, 2017.
- [24] B. H. Ong, E. S. C. Chee, A. Hamid, and K. P. Lim. “Synthesis and Characterization of Nickel Ferrite Magnetic Nanoparticles by Co- Precipitation Method.” *American*

- Institute of Physics.,vol.22, no.12, pp.221-229, 2018.
- [25] M. Ishaque, M.U. Islam, M.A. Khan, I.Z. Rahman, A. Genson, S. Hampshire, “ Synthesis, electrical and dielectric properties of yttrium substituted nickel ferrite.” Journal of Physics B: Condensed Matter. vol. 405, pp.1532-1540, 2010.
- [26] M. Grigorova, H.J. Blythe, V. Blaskov, V. Rusaniv, V. Petkov, V. Masheva, D. Nitianova, L.M. Martinez, J.S. Muñoz, M. Mikhov, “ Magnetic properties and Mossbouer spectra of nanosized  $\text{CoFe}_2\text{O}_4$ .” Journal of Magnetism and Magnetic Materials.,vol.183 pp.163, 1998.
- [27] K. Ishino, Y. Narumiya, Ceram. Bull. “Synthesis, x-ray diffraction and optical band gap study of nanoparticles of  $\text{NiFe}_2\text{O}_4$ .” Journal of pure and applied physics., vol. 66, pp.1469, 1987.
- [28] M. Kamel Attar Kar . “The effect of cationic surfactant on the structure, morphology and optical band gap of ferrites synthesized by a microwave sol-gel auto-combustion method.” Journal of Nano chemical Research., vol. 2, no.2, pp.159-165, 2017.
- [29] E. Souza, J. Duque, L. Kubota and C. Meneses. “Synthesis and characterization of  $\text{NiO}$  and  $\text{NiFe}_2\text{O}_4$  nanoparticles obtained by a sucrose-based route.” Journal of Physics and Chemistry of Solids., vol. 68, pp. 594–599, 2007.
- [30] A. Arif Khan et al. “Influence of preparation method on structural, optical and magnetic properties of nickel ferrite nanoparticles.” Journal of Materials Science., vol. 35, no.1, pp.58-65, 2017.
- [31] R. Suresh, P. Moganavally and M. Deepa. “Synthesis and Characterization of Nickel ferrites nanoparticles.” International Journal of ChemTech Research.,vol. 8, no.5, pp.113-116, 2015.
- [32] D. H. Bobade, S. M. Rathod, and M. L. Mane, “Sol-gel auto-combustion synthesis, structural and enhanced magnetic properties of  $\text{Ni}^{2+}$  substituted nanocrystalline Mg-Zn spinel ferrite,” Journal of Physics B Condensed Matter, vol. 407, no. 18, pp. 3700–3704, 2012.
- [33] S. Shafiee, “Effect of zinc, magnesium, and copper substitutions on the initial permeability of nickel ferrite,” pp. 1–17.
- [34] Shimelis Adem Abegaz. “Sol-gel Combustion Synthesis, Structural and Optical Band Gap Energy Study of  $\text{Zn}_{0.85}\text{Ni}_{0.1}\text{Mg}_{0.05}\text{Fe}_2\text{O}_4$  Nanoparticles.” International

- Research Journal of Engineering and Technology., vol.27, pp.14-19, 2019.
- [35] Carlos Andrés Palacio Gómez, César Augusto BarreroMeneses, ArnaldoMatute, “Structural parameters and cation distributions in solid state synthesized NiZn ferrites.” *Journal of Material Science and Engineering.*,vol.236-237, pp. 48-55, 2018.
- [36] Shannon A. Morrison, Christopher L. Cahill, Everett E. Carpenter, Scott Calvin, Raja Swaminathan, “Magnetic and structural properties of nickel zinc ferrite nanoparticles synthesized at room temperature.” *Journal of Applied Physics.*, vol.95, no 11, 2004.
- [37] Abbasher M Gismelseed, K A Mohammed, H M Widatallah, A D Al-Rawas, M E Elzain and A AYousif “Structure and magnetic properties of the  $Zn_xMg_{1-x}Fe_2O_4$  ferrites,” *Journal of Physics.*, vol. 217, pp. 012138, 2010.
- [38] H. V. Jamadar, M. B. Shelar, M. R. Bhandare, A. M. Shaikh, and B. K. Chougule, “Magnetic Properties of Nanocrystalline Nickel Zinc Ferrites Prepared by Combustion Synthesis.” *International Journal of Self Propagating High Temperature Synthesis. Vol. 20, No. 2, pp. 118–123, 2011.*
- [39] KandasamyVelmurugan, VellaiyappanSangliKaruppananVenkatachalapathy, SechassalomSendhilnathan, “Synthesis of Nickel Zinc Iron Nanoparticles by Coprecipitation Technique”. *Journal of Materials Research.*, vol.13, n.3, pp.299-303, 2010.
- [40] S. Kasap. “Elements of X-Ray diffraction by crystals.” *Journal of materials.*, vol.1, no.1, pp.1-13, 2001.
- [41] S. Sagadevan, Z. Z. Chowdhury, R. F. Rafique, and N. Brunswick. “Preparation and Characterization of Nickel ferrite Nanoparticles via Co-precipitation Method.” *Journal of Materials Research.*, vol.21, no.18, pp.21-25, 2018.
- [42] Alyamani and O. M. Lemine, “Field Emission Scanning Electron Microscopy( FE-SEM) of some nanomaterials.”, 2011.
- [43] W. M. Doyle, “Principles and Applications of Fourier Transform Infra- red ( FTIR ) Process Analysis.”
- [44] T. Nicolet and C. All, “Introduction to Fourier Transform Infrared Spectrometry,” 2001.
- [45] M. S. A. Rani, N. S. Mohamed, and M. I. N. Isa, “Investigation of the Ionic Conduction Mechanism in Carboxymethyl Cellulose/Chitosan Biopolymer Blend

- Electrolyte Impregnated with Ammonium Nitrate,” *International Journal of Polymer Analysis and Characterization.*, vol. 20, no. 6, pp. 491–503, 2015.
- [46] V. Lopez-dominguez, A. Quesada, and J. Spottorno, “A simple Vibrating Sample Magnetometer for macroscopic samples,” April, 2018.
- [47] C. Ehi-eromosele, B.I. Ita, E.E. Iweala, S.A. Adalikwu, P.A. Lanawe, “Magneto-structural properties of Ni–Zn nanoferrites synthesized by the low-temperature auto-combustion method.” *Bulletin of Materials Science*, vol. 38, No. 5, pp. 1465–1472, 2015.
- [48] H.S.C. O’Neill, A. Navrotsky, “Simple spinels; crystallographic parameters, cation radii, lattice energies, and cation distribution”, *American Mineralogist*, vol, 68, pp.181–194, 1983.
- [49] S.M.Chavan, M.K.Babrekar, S.S.More, K.M.Jadhav, “Structural and optical properties of nanocrystalline Ni–Zn ferrite thin films.” *Journal of Alloys and Compounds*, Vol.507, No. 1, pp. 21-25, 2010.
- [50] S.B. Somvanshi, M.V. Khedkar, P.B. Kharat, K.M. Jadhav, “Influential diamagnetic magnesium ( $Mg^{2+}$ ) ion substitution in nano-spinel zinc ferrite ( $ZnFe_2O_4$ ): Thermal, structural, spectral, optical and physisorption analysis.” *Ceramics International*, Vol. 46, No. 7, pp. 8640-8650, 2020.
- [51] B. Senthilkumar, R. KalaiSelvan, P. Vinothbabu, I. Perelshtein, A. Gedanken, “Structural, magnetic, electrical and electrochemical properties of  $NiFe_2O_4$  synthesized by the molten salt technique.” *Materials Chemistry and Physics*, vol. 130, pp. 285–292. 2011.
- [52] H. Moradmard, S.F. Shayesteh, P. Tohidi, Z. Abbas, M. Khaleghi, “Structural, magnetic and dielectric properties of magnesium doped nickel ferrite nanoparticles.” *Journal of Alloys and Compounds*, vv. 650, pp. 116-122, 2015.
- [53] M. Dhiman, A. Goyal, V. Kumarb, S. Singhal, “Designing different morphologies of  $NiFe_2O_4$  for tuning of structural, optical and magnetic properties for catalytic advancements.” *New Journal of Chemistry*, vol. 40, pp. 10418—10431, 2016.
- [54] S.S. Rao, D. Ravinder, “Composition dependence of elastic moduli of gadolinium-substituted nickel–zinc ferrites.” *Materials Letters*, Vol. 57, No. 24–25, pp. 3802-3804, 2003.

- [55] A. Manikandan, J.J. Vijaya, M. Sundararajan, Meganathan, L.J. Kennedy, M. Bououdina, “Optical and magnetic properties of Mg-doped ZnFe<sub>2</sub>O<sub>4</sub> nanoparticles prepared by rapid microwave combustion method.” *Superlattices and Microstructures* Vol. 64, pp. 118-131, 2013.
- [56] Kh. Roumaih, M. Yehia, H. E. Hassan, “Synthesis and Characterization of Core–Shell NiFe<sub>2</sub>O<sub>4</sub>@MgFe<sub>2</sub>O<sub>4</sub> and ZnFe<sub>2</sub>O<sub>4</sub>@MgFe<sub>2</sub>O<sub>4</sub> Nanoferrites.” *Journal of Inorganic and Organometallic Polymers and Materials*, Vol. 30, pp. 3132–3142, 2020.

